Optimized Data Sampling and Energy Consumption in IIoT: A Federated Learning Approach

Yung-Lin Hsu, *Student Member, IEEE*, Chen-Feng Liu, *Member, IEEE*, Hung-Yu Wei, *Senior Member, IEEE*, and Mehdi Bennis, *Fellow, IEEE*

***Abstract*—Real-time environment monitoring is a key application in Industrial Internet of Things, where sensors proactively collect and transmit environmental data to the controller. However, due to limited wireless resources, keeping sensors' sampled data fresh at the controller is critical. This work aims to investigate the trade-off between the sensor's data-sampling frequency and long-term data transmission energy consumption while maintaining information freshness. Leveraging the entropic risk measure (ERM), we jointly minimize the global transmission energy's mean and variance subject to probabilistic constraints on information freshness. Furthermore, while jointly saving the model training energy, we adopt the federated learning (FL) paradigm and propose an FL-based two-stage iterative optimization framework to optimize the aforementioned objective. Specifically, we iteratively learn the sampling frequency via Bayesian optimization and minimize the long-term ERM of the global energy consumption via Lyapunov optimization. Numerical results show that the proposed FL-based scheme saves substantial executing energy with less performance loss. Quantitatively, compared with the centralized learning baseline, the proposed FL-based framework saves up to 69% model training energy at the expense of a mere increased objective outcome, i.e., 6.3% in the global data transmission energy consumption (9.936×10^{-5} in ERM) under 0.4% bias from the global optimal data-sampling frequency.**

***Index Terms*—5G and beyond, industrial Internet of Things (IIoT), federated learning, age of information (AoI), extreme value theory.**

I. Introduction

INDUSTRIAL Internet of Things (IIoT), among the mission-critical applications in 5G networks and beyond, is a key enabler for the real-time monitoring and control of the environmental status in factory automation. In IIoT, intelligent devices such as sensors, meters, and monitors dynamically record the status data and upload them to the central controller (in control systems). To further enhance the performance of factory automation, predictive and prescriptive analysis provides a means in which sensors can proactively record and upload the dynamics of environmental factors to a controller [2]. However, the freshness or staleness of the controller's available data (obtained from the sensors) will affect the system performance of factory automation. In this regard, since the environmental status, e.g., temperature, varies dynamically, the controller's information may deviate from the real-time status if the sampled data cannot be updated in time from the perspective of the controller. If the deviation grows unexpectedly over time, the performance of real-time environment monitoring will be poorly degraded [3]. In order to address the information staleness concerns, Kaul *et al.* introduced the metric, *age of information* (AoI) [4], which measures the elapsed time since the data was sampled/generated by a sensor until being received at the controller. A frequent data sampling may keep the AoI small, whereas excessive sampled data will overwhelm the sensor's transmission system. Due to the limited communication resources (e.g., transmit power), the trade-off between the status-sampling frequency and the transmission energy of the sampled data becomes a critical issue. The impacts of resource allocation on the AoI performance have been investigated in various communication systems [5]–[18].

This work was supported in part by the Ministry of Science and Technology (MOST) of Taiwan under the Graduate Students Study Abroad Program grant 109-2917-I-002-007, and grant 111-2221-E-002-097-MY3, in part by the CHIST-ERA project CONNECT, in part by the CHIST-ERA project LeadingEdge, in part by the EU-H2020 project IntellIoT, and in part by the the Nokia Bell Labs project NEGEIN. This paper was presented in part at the IEEE International Symposium on Personal, Indoor and Mobile Radio Communications, September 2021 [1].

Yung-Lin Hsu and Hung-Yu Wei are with the Graduate Institute of Communication Engineering, National Taiwan University, Taipei 10617, Taiwan (e-mail: d04942010@ntu.edu.tw; hywei@ntu.edu.tw).

Chen-Feng Liu is with the Technology Innovation Institute, 9639 Masdar City, Abu Dhabi, United Arab Emirates (e-mail: chen-feng.liu@tii.ae).

Mehdi Bennis is with the Centre for Wireless Communications, University of Oulu, 90014 Oulu, Finland (e-mail: mehdi.bennis@oulu.fi).

A. Related Work

To minimize the sensors' power consumption subject to the constraints on the maximal AoI's tail behavior, the work [5] considered a centralized instruction-issuing scheme for sampling and uploading the environmental data in a multi-sensor IIoT system. By focusing on a dense IoT monitoring system [6], Zhou and Saad proposed a mean-field game approach to minimize the average AoI and average peak AoI subject to the average energy constraint. The authors further considered a noisy-channel contention-based IoT monitoring system. While discussing the cases with and without transmission feedback, they proposed three policies and characterized the closed-form expressions of the average AoI [7]. The work [8] investigated the average peak AoI with deadlines in IoT networks. Therein, the closed-form expressions of the AoI distributions were derived. To optimize the average peak AoI, the authors in [9] modeled the procedure of computing and transmission as a tandem queue and formulated a min-max optimization problem to optimize the packet-updating rate. A half-duplex transmission and wireless energy harvesting scenario was investigated in [10]. Therein, the authors aimed to minimize the AoI while considering the waiting time for

energy harvesting. Additionally, the work [11] considered a remote monitoring problem that trades off the average AoI and the AoI threshold violation probability.

Moreover, some works used Markov decision processes (MDPs) to study the AoI problems in various communication systems. The authors in [12] investigated the trade-off between the AoI and energy cost and proposed an action policy for the devices. In addition, the work [13] constructed a learning-based AoI-optimal policy which jointly accounts for the time and (consumed and harvested) energy to update the status from the source nodes. A status-updating policy was studied and designed in a multi-packet IoT system [14]. This work jointly considered the sampling and the scheduling mechanisms for minimizing the average AoI. The work [15] considered a single-destination multi-device computation-enabled IoT system. To minimize the average weighted sum of the AoI and energy consumption, the authors proposed the joint offloading and scheduling policies. Additionally, Tang *et al.* [16] proposed the scheduling algorithms to minimize the average AoI under time-varying channels. Yin *et al.* [17] focused on a correlated AoI optimization problem in the IoT systems and further proposed a learning-based approach. In the work [18], the authors proposed the deep reinforcement learning-based policies to optimize the weighted average of the AoI and throughput in the wireless energy transfer systems. In the nutshell, the work with game-theoretic approaches [5], [6] or MDP-based approaches [12]-[17] considered steady-state solutions with discrete system conditions and policies/actions. Furthermore, the considered AoI or data staleness were discretized.

Centralized optimization and centralized learning (CL) have been widely used to improve the system performances of the AoI, data transmission energy, etc. for real-time monitoring [5], [13], [15]–[18]. However, CL consumes significant training energy while computing the collected global raw data in a centralized manner and may take considerable transmission energy for delivering large size raw data. In contrast, federated learning (FL) [19]–[22], a decentralized and collaborative paradigm, emerged as an alternative for model training, which trains a global model by leveraging local model training across sensors [20], [21], [23]. Compared with CL, the benefits of energy saving in FL paradigms were discussed in [20], [21], [24], [25], and numerically investigated in [26]. The trade-off between the communication cost and the protection of the privacy-sensitive data was investigated in [27]. Therefore, the aforementioned AoI works [5], [13], [15]–[18], which suppressed the AoI in a centralized manner, implicitly incurred tremendous signaling overheads and energy consumption. The authors in [28] focused on a scheduling policy for FL in a wireless system, which jointly accounts for the AoI of the local device's model updates and the instantaneous wireless channel quality. Additionally, some works were dedicated on the FL performance improvement. In [29], part of the local-model training, which is carried out by local devices, is split into the edge server to improve the learning efficiency and decrease the global communication frequency. For real-time data analysis in IoT scenarios, the authors in [30] combined edge and cloud computing, which leads to reductions up to 80% in exchanged data between the edge and cloud by feature learning. Finally, the authors in [31] proposed a local-model selection approach accounting for the correlation in the sensor's training data in an IIoT scenario. Their goal was to dynamically optimize the power for delivering the environmental data. In our previous work [1], we considered a fixed data-sampling rate scenario and proposed an FL-based approach. The proposed solution could real-time dynamically optimize the data transmit power with the uncertainty of the channel condition. The objective was to minimize the long-term risk-sensitive global sampled data transmission energy subject to data staleness and extremely large AoI constraints. Therein, each sensor locally learns the AoI of the uploaded data and regresses the extreme AoI exceedances model. For extreme AoI model regression, we further adopted FL to improve the accuracy.

B. Our Contribution

Inheriting from our previous work [1], in this work, we consider a multi-sensor IIoT system and study a controller-sensor collaborative scheme. Subject to the probabilistic and extreme AoI/data staleness constraints, our objective is to optimize the trade-off between the data-sampling frequency (by adjusting the sampling criterion at the sensor side) and the global long-term risk-sensitive transmission energy of sending the sampled data.

Therein, the channel condition and the data-sampling time instance in the studied scenario vary over time at different sensors, making the transmission energy allocation nontrivial and thus causing the AoI/data staleness. To achieve the objective, we propose a dynamic transmit power and sampling frequency optimization policy by marrying tools from Lyapunov optimization [32], extreme value theory (EVT) [33], and Bayesian optimization (BO) [34]. We further regress the distribution of the extreme staleness cases (i.e., the data with a very large AoI) to the generalized Pareto distribution (GPD) models in order to optimize the transmission energy. Moreover, since the individual accuracy of the GPD-model regression is limited due to the lack of the extreme-AoI data at the sensors, we leverage FL not only for mitigating the deviation among the sensors' model regression but also for training-energy saving. In contrast with our previous work [1], the unique contributions of this paper are listed as follows:

- We propose a top-down system design to trade off the data-sampling frequency and data transmission energy.
  - The data-sampling frequency can be optimized to balance the requirements of the general and specific extreme data staleness/AoI and the tense of data transmission.
  - Instead of seeking the steady-state performance of the AoI, e.g., game-theoretic approaches [6], [7] or MDP-based approaches [13]–[18], we meet the long-term data staleness constraints by dynamically optimizing the transmit power of each sampled data, gaining more resilience to deal with the variation of the channel condition.

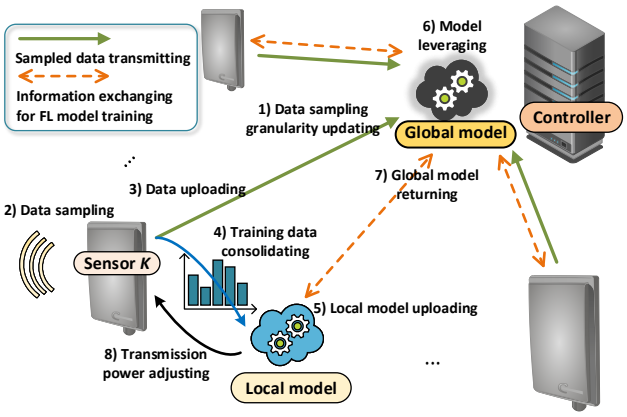

Figure 1: Controller-sensor collaborative FL-based scenario

  - For extreme staleness/AoI constraint fulfillment, we not only consider preventing the individual occurrence as in [1] but also propose an improved apportion scheme which allows the staleness/AoI to be continuous.
- We propose an FL-based two-stage iterative optimization framework for computation energy saving.
  - In the first stage, the controller learns the optimal data-sampling frequency by BO.
  - In the second stage, each sensor optimizes the transmission energy of the sampled data under a given sampling frequency by leveraging Lyapunov optimization and EVT.
  - Via numerical results, we examine the energy-saving benefits of the proposed FL-based scheme for model training and the cost minimization (which incorporates the data-sampling frequency, risk-sensitive energy consumption, and satisfaction of data freshness constraints) over the CL scheme.

The remainder of this paper is organized as follows. The system model and problem formulation are specified in Section II. In Section III, we illustrate the proposed two-stage framework of the data-sampling frequency and long-term transmission energy allocation. The numerical results and the performance of the proposed scheme are shown and discussed in Section IV. Finally, this work is concluded in Section V.

II. System Model and Problem Formulation

A. System Architecture

As shown in Fig. 1, we consider an IIoT network which contains a controller and a set $\mathcal{K}$ of K wireless sensors for environment monitoring. Sensors separately monitor the status of distinct and independent (but of the same type) environmental changes. After the sensor samples an environmental status data, the data is transmitted immediately to the controller if the uploading procedure (of all the previous data) has been completed. Otherwise, new data is queued in the buffer. Moreover, we imbue FL into the considered IIoT system for enhancing the data freshness and optimizing the transmission energy, which will be elaborated in Section III.

We assume that the data sampling is event-triggered. Each sensor will sample a new data if the experienced change of the environmental status is larger than a value $C_g \in \mathbb{R}^+$. The value of C_g also reflects the data-sampling frequency. A smaller/larger C_g implies that the sensors need to sample the data more/less frequently. For each sensor $k \in \mathcal{K}$, its sampled data are indexed by $i \in \mathbb{Z}^+$. Here, we denote the data sampled by a sensor, which follows C_g, as $(i|C_g)$. To send the i-th environmental data with D_{env} bits, sensor k allocates a transmit power $p_k(i|C_g)$ with a transmission delay

$$t_k(i|C_g) = \frac{D_{env}}{B\log_2\left(1+\frac{h_k(i|C_g)p_k(i|C_g)}{BN_0}\right)}. \tag{1}$$

Here, $h_k(i|C_g)$ is the channel gain with path loss which changes with time between sensor k and the controller. B is the dedicated bandwidth to sensor k while N_0 is the power spectral density of the additive white Gaussian noise. The environmental data sampling and the AoI function of sensor k are schematically illustrated in Fig. 2. Note that the AoI of each data measures the elapsed time since the data was sampled by a sensor until being received at the controller. In Fig. 2, H_k is the experienced continuous environmental changes of sensor k. Therein, $\tau_k(i|C_g)$ represents the sensor k's i-th data-sampling time instant, and $b_k(i|C_g) = \tau_k(i|C_g) - \tau_k(i-1|C_g) > 0, \forall\, i = 2, 3, \cdots$, is the sampling time interval between the $(i-1)$-th data and the i-th data. The interval $b_k(i|C_g)$ varies with the uncertain environmental changes and the sampling criterion C_g. Additionally, the queuing time $q_k(i|C_g)$ is caused by the AoI of the previous, i.e., $(i-1)$-th, data $a_k(i-1|C_g)$ if it has not been delivered to the controller yet. We can straightforwardly find

$$q_k(i|C_g) = [a_k(i-1|C_g) - b_k(i|C_g)]^+,\ \forall\, i \in \mathbb{Z}^+, \tag{2}$$

which varies for each data, with $[\cdot]^+ = \max(\cdot, 0)$. Accordingly, the AoI of the i-th data $a_k(i|C_g)$ is composed of the queuing time $q_k(i|C_g)$ and its transmission time $t_k(i|C_g)$, i.e., $a_k(i|C_g) = q_k(i|C_g) + t_k(i|C_g)$. The AoI is also dynamic and can be expressed in a recursive manner as

$$a_k(i|C_g) = [a_k(i-1|C_g) - b_k(i|C_g)]^+ + t_k(i|C_g),\ \forall\, i \in \mathbb{Z}^+. \tag{3}$$

B. Problem Formulation

For real-time monitoring, a smaller C_g increases the sampling frequency but accumulates more sampled data to be delivered. Due to transmission staleness, obsolete data (i.e., data with a high AoI) may significantly degrade the overall performance. Thus, we impose additional constraints on the AoI as follows. To emphasize the criticality of the AoI, we firstly introduce a *staleness function* [28], [35]

$$f_k(i|C_g) = \frac{[a_k(i|C_g)]^2}{2},\ \forall\, i \in \mathbb{Z}^+, k \in \mathcal{K}. \tag{4}$$

Then, under a given C_g, we consider a long-term time-averaged staleness constraint

$$\overline{f}_k(C_g) = \lim_{I\to\infty} \frac{1}{I}\sum_{i=1}^{I} \mathbb{E}[f_k(i|C_g)] \le f_m,\ \forall\, k \in \mathcal{K}, \tag{5}$$

This article has been accepted for publication in IEEE Transactions on Communications. This is the author's version which has not been fully edited and content may change prior to final publication. Citation information: DOI 10.1109/TCOMM.2022.3216353

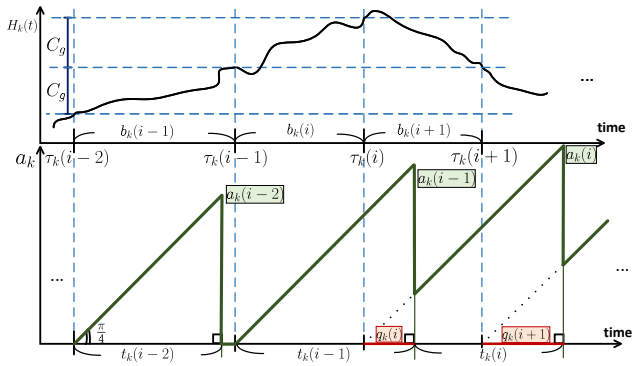

Figure 2: Illustrations of the status changes $H_k(t)$, data-sampling sensitivity C_g, queuing time $q_k(i)$, and AoI $a_k(i)$. In this case, the $(i-2)$-th and $(i-1)$-th data can be uploaded immediately. Thus, both $q_k(i-2)$ and $q_k(i-1)$ are zero.

for every sensor in which f_m is the threshold. Here, I represents the total transmission times in the communication timeline. Additionally, we consider a probabilistic constraint on the occurrence of extreme staleness

$$\overline{Pr}_k(C_g) = \Pr\{f_k(i|C_g) > f_{es}\} \leq \epsilon_{es},\ \forall\, i \in \mathbb{Z}^+,\ \forall\, k \in \mathcal{K}, \tag{6}$$

where $f_{es} > 0$ is the threshold of extreme staleness, and $\epsilon_{es} \ll 1$ is the tolerable occurrence probability. Furthermore, if the extreme staleness grows drastically, the real-time monitoring performance of the system will degrade. Hence, we further impose a probabilistic constraint on the event of extreme staleness exceedances

$$\begin{aligned}\overline{Pr}_k^{(ex)}(C_g) = \Pr\{f_k(i|C_g) > f_{es} + f_{ea} \big| f_k(i|C_g) > f_{es}\} \\ \leq \epsilon_{ea},\ \forall\, i \in \mathbb{Z}^+,\ \forall\, k \in \mathcal{K}.\end{aligned} \tag{7}$$

Here, $f_{ea} > 0$ is the threshold of staleness exceedances, and ϵ_{ea} is the tolerable probability. Conditioned on the extreme staleness events (i.e., the staleness value $f_k(i|C_g)$ which is greater than the threshold f_{es}), constraint (7) enforces that the occurrence probability of the staleness data which additionally violate another threshold f_{ea} should be less than ϵ_{ea}.

Taking the sensors' limited-energy concerns into account, we aim to jointly minimize the data-sampling frequency (in terms of C_g) and sensors' long-term transmission energy consumption subject to the imposed staleness constraints. Note that even though the sensors monitor the same type of environments, the numbers of sampled data (and total energy consumption) of different sensors are distinct due to the uncertainty of the individual experienced status changes. In order to mitigate the deviation of data transmission energy among sensors, we invoke the entropic risk measure (ERM) $\frac{1}{\rho}\ln(\mathbb{E}_X[\exp(\rho X)])$ to jointly incorporate the mean and variance/deviation [36]. Note that the risk-sensitivity parameter $\rho > 0$ reflects the weights of variance and higher-order statistics of the random variable X. Thus, denoting the sensor k's consumed energy for sending its i-th data as $E_k(i|C_g) = p_k(i|C_g)t_k(i|C_g)$, we formulate the studied optimization problem as follows:

$$\underset{p_k(i|C_g), C_g}{\text{minimize}}\ \alpha C_g + \sum_{k\in\mathcal{K}} \frac{1}{\rho} \ln\left(\lim_{I\to\infty} \frac{1}{I}\sum_{i=1}^{I} \exp\left(\rho E_k(i|C_g)\right)\right) \tag{8a}$$

$$\text{subject to}\ \ 0 \leq p_k(i|C_g) \leq p_{max},\ \forall\, i \in \mathbb{Z}^+, k \in \mathcal{K}, \tag{8b}$$

$$C_g > 0, \tag{8c}$$

$$(5) - (7),$$

in which p_{max} is the sensor's power budget. Additionally, $\alpha > 0$ trades off the criterion value (for the data-sampling frequency) and the entropic risk measure of energy consumption.

III. Data Staleness-Aware Power Allocation

Note that in problem (8), the value of C_g affects the network-wide energy consumption and the staleness of sampled data. However, since the environmental status (i.e., H_k in Fig. 2) varies randomly and individually at each sensor, the impacts of C_g on the energy consumption and data staleness are unknown for solving problem (8).

To address this issue while saving the model training computation energy (as the highlighted advantages in Section I), we adopt the FL paradigm and propose a *FL-based two-stage sampling-frequency and energy trade-off scheme* (FLTS-SETOS). In the first stage, with a given C_g from the controller (estimated as the most potential value to improve the system performance), the sensors sample the environmental data accordingly and transmit them to the controller. Therein, the sensors optimize the sampled data transmit power with the proposed *Lyapunov-based iterative transmission optimization scheme* (Lya-ITOS) and feed back the statistical results of the ERM energy consumption (the second term in (8a)) to the controller. In the second stage, the controller iteratively learns the value of C_g using *BO-based via a sampling criterion optimization scheme* (Bay-SCOS) according to the historical results (such as the global ERM energy consumption results and the satisfaction level of the constraints.) To detail the sensors-controller cooperative scheme, FLTS-SETOS, in Section III-A, we present Lya-ITOS with a given C_g. Subsequently, we demonstrate the optimal C_g-value estimation algorithm, Bay-SCOS, in Section III-B.

A. Lyapunov-Based Iterative Transmission Optimization Scheme (Lya-ITOS)

With a controller-selected C_g, the entropic risk measure minimization of the transmission energy is given as

$$\begin{aligned}\underset{0\leq p_k(i|C_g)\leq p_{max}}{\text{minimize}}\ \ & \sum_{k\in\mathcal{K}} \frac{1}{\rho} \ln\left(\lim_{I\to\infty} \frac{1}{I}\sum_{i=1}^{I} \exp\left(\rho E_k(i|C_g)\right)\right) \\ \text{subject to}\ \ & (5) - (7).\end{aligned} \tag{9}$$

Note that for notational simplicity, we neglect C_g in problem (9) and throughout Section III-A. Here, constraint (7) concerns the exceedances of extreme staleness which is rooted in the tail distribution of the staleness f_k. In this regard, EVT provides

a powerful tool to characterize the tail behavior of the general probability distribution as shown in Theorem 1.

Theorem 1 (**Pickands–Balkema–de Haan Theorem** [33])**.** *Given a random variable X, the complementary cumulative distribution function (CCDF) of the exceedance over a threshold $Y|_{X>d_0} = X - d_0$ can be approximated as a GPD, i.e.,*

$$F_Y(y) = \Pr(X \geq y + d_0 | X > d_0) \approx \left(1 + \frac{\xi y}{\sigma}\right)^{-1/\xi},$$

when the threshold $d_0 \to F_X^{-1}(1)$. The GPD is characterized by a scale parameter $\sigma > 0$ and a shape parameter $\xi \in \mathcal{R}$.

By applying the results in Theorem 1 to (7), we have

$$\Pr\{f_k(i) - f_{ea} \geq f_{es} | f_k(i) > f_{es}\} = \left(1 + \frac{\xi f_{ea}}{\sigma}\right)^{-1/\xi} \leq \epsilon_{ea}.$$

Note that the GPD parameters (σ, ξ) for the conditional extreme staleness constraint (7) are not available beforehand but can be learned from the sensors' individual empirical extreme staleness data (experienced in the previous time slots) by GPD distribution model regression (which will be detailed in Section III-A2 and III-A3.) Hence, to deal with problem (9), Lya-ITOS is an M-iteration scheme to seek the optimal solution. In each iteration (indexed by m), we use two sub-schemes. The first one, *Lyapunov-based transmission energy optimization* (L-TEO), leverages Lyapunov optimization to optimize the sampled data transmission energy subject to constraints (5) and (6). The second sub-scheme, *GPD model-based transmission energy enhancement* (GPD-TEE), trains the GPD model with the extreme staleness data consolidated from the first sub-scheme, and further optimizes the data transmit power under constraint (7). The operations of the two sub-schemes in each iteration are described as follows.

1) Lyapunov-Based Transmission Energy Optimization (L-TEO): In the (m)-th iteration, we exclude constraint (7) and focus on the following problem. For sensor k, the individual problem becomes

$$\begin{aligned} \underset{p_k(i|C_g)}{\text{minimize}} \quad & \lim_{I\to\infty} \frac{1}{I} \sum_{i=1}^{I} \exp\left(\rho E_k(i)\right) \\ \text{subject to} \quad & (5), (6), \text{and } (8b), \end{aligned} \tag{10}$$

in which we consider $\exp\left(\rho E_k(i)\right)$ as the objective since $\frac{1}{\rho}\ln(\cdot)$ in (8a) is a monotonically increasing function. Utilizing Lyapunov optimization, we solve the long-term time-averaged problem as follows. First of all, scaling both sides of (6) by $f_k(i)$ and incorporating $\Pr\{f_k(i) > f_{es}\} = \mathbb{E}[\mathbb{1}_{\{f_k(i)>f_{es}\}}]$, we rewrite (6) as

$$\lim_{I\to\infty} \frac{1}{I} \sum_{i=1}^{I} f_k(i) \mathbb{E}[\mathbb{1}_{\{f_k(i)>f_{es}\}}] \leq \lim_{I\to\infty} \frac{1}{I} \sum_{i=1}^{I} f_k(i) \epsilon_{es}, \tag{11}$$

where $\mathbb{1}_{\{\cdot\}}$ is the index function. Then, we introduce two virtual queues, which evolve as

$$\Gamma_k(i+1) = [\Gamma_k(i) + f_k(i) - f_m]^+, \tag{12}$$

$$\Lambda_k(i+1) = [\Lambda_k(i) + (\mathbb{1}_{\{f_k(i)>f_{es}\}} - \epsilon_{es}) f_k(i)]^+, \tag{13}$$

for constraints (5) and (6), respectively. Subsequently, by applying $([x]^+)^2 \leq x^2$, we straightforwardly derive an upper bound on the conditional Lyapunov drift-plus-penalty for the i-th data transmission as (14), in which $V > 0$ is the parameter to trade off the virtual queue suppression and energy consumption optimality in (10). Note that the time-averaged constraints are satisfied if the corresponding virtual queues are stabilized over time [32]. Hence, to optimize the objective in (10) and ensure the stability of the virtual queues of the corresponding constraints, we minimize the upper bound (14) in each data transmission $i \in \mathbb{Z}^+$. To this end, each sensor k solves

$$\underset{0\leq p_k(i)\leq p_{max}}{\text{minimize}} \quad \chi_k'(i) f_k^2(i) + \chi_k''(i) f_k(i) + V \exp\left(\rho E_k(i)\right) \tag{15}$$

with $\chi_k'(i) = \frac{1}{2}(1 + \mathbb{1}_{\{f_k(i)>f_{es}\}} + \epsilon_{es}^2)$ and $\chi_k''(i) = (\Gamma_k(i) + \Lambda_k(i)\mathbb{1}_{\{f_k(i)>f_{es}\}})$ to allocate the transmit power $p_k(i|C_g)$ for its i-th transmission. Note that $\chi_k'(i) f_k^2(i) + \chi_k''(i) f_k(i)$ is convex, whereas $\exp\left(\rho E_k(i)\right)$ is non-convex with respect to $p_k(i)$. In order to tractably find a solution to the non-convex problem (15), we adopt the notion of the convex-concave procedure (CCP) [37] in which the non-convex function $\exp\left(\rho E_k(i)\right)$ is iteratively convexified by the first-order Taylor series expansion with respect to a feasible reference point $\hat{p}_k$, i.e.,

$$\begin{aligned} &\exp\left(\rho E_k(\hat{p}_k)\right) \\ &\times \left[t_k(\hat{p}_k) \left(1 - \frac{\hat{p}_k h_k t_k(\hat{p}_k)}{D_{env}(\hat{p}_k h_k + N_0 B)\ln 2}\right)(p_k - \hat{p}_k) + 1 \right]. \end{aligned}$$

Specifically, given the reference point $\hat{p}_k^r$ in the r-th iteration of the CCP, we focus on the convexified problem

$$\underset{0\leq p_k^{r+1}\leq p_{max},}{\text{minimize}} \quad \chi_k' f_k^2(p_k^{r+1}) + \chi_k'' f_k(p_k^{r+1}) + V J(\hat{p}_k^r) p_k^{r+1} \tag{16}$$

with $J(\hat{p}_k^r) = \exp(\rho E_k(\hat{p}_k)) t_k(\hat{p}_k^r)\left[1 - \frac{\hat{p}_k^r h_k t_k(\hat{p}_k^r)}{D_{env}(\hat{p}_k^r h_k + N_0 B)\ln 2}\right]$. Here, we ignore the data index i. By differentiation, the optimal solution to (16) is given by $(p_k^{r+1})^\star = \max\{\min\{\tilde{p}_k^{r+1}, p_{max}\}, 0\}$ in which $\tilde{p}_k^{r+1}$ satisfies

$$\begin{aligned} &-\left\{ \chi_k' \left[q_k + \frac{D_{env}\ln 2}{B \ln\left(1 + \frac{h_k \tilde{p}_k^{r+1}}{BN_0}\right)} \right]^3 \right. \\ &\qquad \left. + \chi_k'' \left[q_k + \frac{D_{env}\ln 2}{B \ln\left(1 + \frac{h_k \tilde{p}_k^{r+1}}{BN_0}\right)} \right] \right\} \\ &\times \left(\frac{D_{env} h_k \ln 2}{N_0 \left[\ln\left(1 + \frac{h_k \tilde{p}_k^{r+1}}{BN_0}\right) \right]^2 \left(1 + \frac{h_k \tilde{p}_k^{r+1}}{BN_0}\right)} \right) + V J(\hat{p}_k^r) = 0. \end{aligned}$$

The solution in the r-th iteration is then set as the reference point of the next iteration $r+1$, i.e., $\hat{p}_k^{r+1} = (p_k^{r+1})^*$. After a sufficient number of CCP iterations, sensor k uses the converged solution as $(p_k^{(m)})^*(i) = (p_k^\infty)^*$ in the L-TEO (m)-th iteration. Note that $(p_k^{(m)})^*(i)$ is the solution subject to constraints (5) and (6) only. The actual energy for data transmission is tuned with the empirical results $(\Delta p_k^{(m-1)})^*$ of GPD-TEE in the previous (i.e., $(m-1)$-th) iteration in order to meet constraint (7). The proposed GPD-TEE is illustrated as follows.

This article has been accepted for publication in IEEE Transactions on Communications. This is the author's version which has not been fully edited and content may change prior to final publication. Citation information: DOI 10.1109/TCOMM.2022.3216353

2) GPD Model-Based Transmission Energy Enhancement (GPD-TEE): In the (m)-th iteration, after preforming L-TEO and collecting considerable empirical data to characterize the GPD parameters, the next step is to adjust the transmit power for the next (i.e., $(m+1)$-th) iteration to satisfy (7). Hereafter, we use the superscript $(\cdot)^{(m)}$ to refer the metrics collected in the (m)-th iteration, e.g., $a_k^{(m)}$, $t_k^{(m)}$, and $f_k^{(m)}$ for the statistical results of a_k, t_k, and f_k, while solving (10). The set of extreme staleness exceedances is denoted by $\mathcal{Q}_k^{(m)} = \{\hat{f}_k^{(m)}(i) = f_k^{(m)}(i) - f_{es} > 0 : i \in \mathbb{Z}^+\}$ which will be further used for training the GPD parameters as explained in Section III-A3.

If the constraint (7) is not satisfied, we decrease the global staleness by an amount $A_{adj}^{(m)} \geq 0$. After the deduction, the CCDF of the staleness exceedances (by applying Theorem 1) is given by

$$\begin{aligned}\Pr_{\{\mathcal{Q}_k^{(m)}\}} &\{\hat{f}_k^{(m)} - A_{adj}^{(m)} > f_{ea}\} \\ &\approx \left(1 + \frac{\xi^{(m)}(A_{adj}^{(m)} + f_{ea})}{\sigma^{(m)}}\right)^{-1/\xi^{(m)}} \leq \epsilon_{ea}, \end{aligned} \quad (17)$$

which can be rewritten as an lower bound on $A_{adj}^{(m)}$, i.e.,

$$A_{adj}^{(m)} \geq A_{min} \equiv \left(\sigma^{(m)}\left[(\epsilon_{ea})^{-\xi^{(m)}} - 1\right]/\xi^{(m)} - f_{ea}\right)^+. \quad (18)$$

After subtracting $A_{adj}^{(m)}$ from the staleness exceedance $\hat{f}_k^{(m)}$, we consider the mean as

$$\begin{aligned}\mathbb{E}_{\{\mathcal{Q}_k^{(m)}\}}\left[\hat{f}_k^{(m)} - A_{adj}^{(m)}\right] &= \mathbb{E}_{\{\mathcal{Q}_k^{(m)}\}}\left[f_k^{(m)} - f_{es} - A_{adj}^{(m)}\right] \\ &= \mathbb{E}_{\{\mathcal{Q}_k^{(m)}\}}\left[\frac{1}{2}\left(a_k^{(m)}\right)^2 - f_{es} - A_{adj}^{(m)}\right]. \end{aligned} \quad (19)$$

Moreover, diminishing the staleness can be done by directly decreasing the data's AoI. In this regard, we reduce the AoI by an interval $\Delta t_k^{(m)}$ of the transmission time and have

$$\begin{aligned}&\mathbb{E}_{\{\mathcal{Q}_k^{(m)}\}}\left[\frac{1}{2}\left(a_k^{(m)}\right)^2 - f_{es} - A_{adj}^{(m)}\right] \\ &\quad = \mathbb{E}_{\{\mathcal{Q}_k^{(m)}\}}\left[\frac{1}{2}(a_k^{(m)} - \Delta t_k^{(m)})^2 - f_{es}\right], \end{aligned} \quad (20)$$

which results in

$$\begin{aligned}A_{adj}^{(m)} = &\frac{1}{2}\left(\mathbb{E}_{\{\mathcal{Q}_k^{(m)}\}}\left[a_k^{(m)}\right]\right)^2 \\ &- \frac{1}{2}\left(\mathbb{E}_{\{\mathcal{Q}_k^{(m)}\}}\left[a_k^{(m)}\right] - \Delta t_k^{(m)}\right)^2. \end{aligned} \quad (21)$$

Then incorporating (18) and (21), we have an lower bound on Δt_k in the feasible real region as

$$\begin{aligned}\Delta t_k^{(m)} \geq \Delta t_{k,min}^{(m)} \equiv &\mathbb{E}_{\{\mathcal{Q}_k^{(m)}\}}\left[a_k^{(m)}\right] \\ &+ \sqrt{\mathbb{E}_{\{\mathcal{Q}_k^{(m)}\}}\left[a_k^{(m)}\right]^2 - 2A_{min}}. \end{aligned} \quad (22)$$

Additionally, we consider the empirical average transmission delay as the longest reducible time, which results in an upper bound

$$\Delta t_k^{(m)} < \bar{t}_k^{(m)} = \mathbb{E}_{\{\mathcal{Q}_k^{(m)}\}}\left[t_k^{(m)}\right]. \quad (23)$$

Given $\tilde{p}_k^{(m)} = g(\exp(\frac{\kappa}{\bar{t}_k^{(m)}}) - 1)$ with $g = BN_0/\bar{h}_k$ and $\kappa = D\ln 2/B$, and denoting the extra transmit power to reduce the time $\Delta t_k^{(m)}$ as $\Delta p_k^{(m)} \geq 0$, we have $\tilde{p}_k^{(m)} + \Delta p_k^{(m)} = g\big(\exp(\frac{\kappa}{\bar{t}_k^{(m)} - \Delta t_k^{(m)}}) - 1\big)$ by following (1). Since we focus on energy consumption in problem (10), we also minimize the energy cost $(\tilde{p}_k^{(m)} + \Delta p_k^{(m)})(\bar{t}_k^{(m)} - \Delta t_k^{(m)})$ while deciding the time reduction, i.e.,

$$\underset{\Delta t_{k,min} \leq \Delta t_k < \bar{t}_k}{\text{minimize}} \; g\big(\exp\left(\frac{\kappa}{\bar{t}_k - \Delta t_k}\right) - 1\big)(\bar{t}_k - \Delta t_k), \quad (24)$$

which is a convex optimization problem. The superscript (m) is emitted in (24) and (25) for notational simplicity. By differentiation, the solution to problem (24) is expressed $\Delta t_k^* = \max\{\min\{\Delta t_k', \bar{t}_k - \delta\}, \Delta t_{k,min}\}$ with $\delta \to 0$ in which $\Delta t_k'$ satisfies

$$\exp\left(\tfrac{\kappa}{\bar{t}_k - \Delta t_k'}\right)\left(1 - \tfrac{\kappa}{\bar{t}_k - \Delta t_k'}\right) - 1 = 0.$$

Accordingly, the increased power derived from the empirical extreme data $\mathcal{Q}_k^{(m)}$ is calculated as

$$\begin{aligned}\Delta p_k^* &= [\tilde{p}_k + \Delta p_k^*] - \tilde{p}_k \\ &= \mu\left(\exp\left(\frac{\kappa}{\bar{t}_k - \Delta t_k^*}\right) - \exp\left(\frac{\kappa}{\bar{t}_k}\right)\right). \end{aligned} \quad (25)$$

Here, we propose two methods to distribute the increased power $(\Delta p_k^{(m)})^*$ to the sensors' transmit power, i.e., the intuitive *extreme staleness power adjustment scheme* (EXT) and the enhanced *apportion power adjustment scheme* (APP).

In EXT, the sensor checks the staleness status at the present iteration $f_k^{(m)}(i)$ of each data before transmission and then increases the transmit power for the data whose staleness

$$\begin{aligned}&\mathbb{E}\Big[\frac{1}{2}\big(\Gamma_k(i+1)\big)^2 + \frac{1}{2}\big(\Lambda_k(i+1)\big)^2 - \frac{1}{2}\big(\Gamma_k(i)\big)^2 - \frac{1}{2}\big(\Lambda_k(i)\big)^2 + V\exp\big(\rho E_k(i)\big)\Big|\Gamma_k(i), \Lambda_k(i)\Big] \\ &\leq \mathbb{E}\Big[\Gamma_k(i)(f_k(i) - f_m) + \frac{1}{2}(f_k(i) - f_m)^2 + \Lambda_k(i)f_k(i)(\mathbb{1}_{\{f_k(i) > f_{es}\}} - \epsilon_{es}) \\ &\quad + \frac{1}{2}f_k^2(i)(\mathbb{1}_{\{f_k(i) > f_{es}\}} - \epsilon_{es})^2 + V\exp\big(\rho E_k(i)\big)\Big|\Gamma_k(i), \Lambda_k(i)\Big] \\ &\leq \mathbb{E}\Big[\frac{1}{2}(1 + \mathbb{1}_{\{f_k(i) > f_{es}\}} + \epsilon_{es}^2)f_k^2(i) + (\Gamma_k(i) + \Lambda_k(i)\mathbb{1}_{\{f_k(i) > f_{es}\}})f_k(i) + \frac{1}{2}f_m^2 + V\exp\big(\rho E_k(i)\big)\Big|\Gamma_k(i), \Lambda_k(i)\Big] \end{aligned} \quad (14)$$

surpasses the threshold f_{es}. In other words, the final transmit power is adjusted as

$$p_{EXT,k}^{(m)}(i) = \begin{cases} \min\left\{(p_k^{(m)})^*(i) + (\Delta p_k^{(m)})^*, p_{max}\right\} \\ \qquad\qquad\qquad\qquad \text{, if } f_k^{(m)}(i) > f_{es}, \\ (p_k^{(m)})^*(i) \qquad\qquad\qquad \text{, otherwise.} \end{cases} \tag{26}$$

Instead of checking the staleness of each transmission, the sensor evenly and proportionally apportions $(\Delta p_k^{(m)})^*$ to every data transmit power in APP, which can shorten the staleness comprehensively. In APP, the transmit power is

$$p_{APP,k}^{(m)}(i) = \min\left\{(p_k^{(m)})^*(i) + \frac{|\mathcal{Q}_k^{(m)}|}{|\mathcal{F}_k^{(m)}|}(\Delta p_k^{(m)})^*, p_{max}\right\}, \tag{27}$$

where $\mathcal{F}_k^{(m)} = \{f_k^{(m)}(i)|\,\forall i\}, \forall\, k \in \mathcal{K}$, is the set of all the staleness-data transmissions in the (m)-th iteration.

Corollary 1. *APP outperforms EXT for extreme staleness cases in the worst-case scenario where the queuing time* (2) *is always non-negative, i.e.,* $q_k(i) = a_k(i-1) - b_k(i) \geq 0, \forall\, i \in \mathbb{Z}^+, k \in \mathcal{K}$, $w.p.\,1$.

Proof. Please refer to Appendix A. □

Finally, after uploading the i-th sampled data with the transmit power in EXT/APP, sensor k updates the virtual queues (12) and (13) as well as the coefficients in (15) for the transmit power in the next $(i+1)$-th data transmission.

3) FL-Based GPD Model Regression: Hereafter, we refer to the characteristic parameters $\theta^{(m)} = (\sigma^{(m)}, \xi^{(m)})$ as the GPD model in the (m)-th iteration. Similarly to our previous work [1], we leverage principles from FL for model training.

At the (m)-th iteration, we aim to find a global GPD model which is the closest to the empirical distribution with respect to the *Kullback–Leibler* (KL) divergence, i.e.,

$$\underset{\theta^{(m)}}{\text{minimize}} \quad G(\theta^{(m)}|\mathcal{Q}^{(m)}) \tag{28}$$

with

$$G(\theta^{(m)}|\mathcal{Q}^{(m)}) = -\sum_{\hat{f}\in\mathcal{Q}^{(m)}} \ln\left(P(\hat{f}|\theta^{(m)})\right).$$

Here, $\mathcal{Q}^{(m)} = \{\mathcal{Q}_k^{(m)} : k \in \mathcal{K}\}$ is the global extreme staleness set while

$$P(\hat{f}|\theta^{(m)}) = \frac{1}{\sigma^{(m)}}\left(1 + \frac{\xi^{(m)}\hat{f}}{\sigma^{(m)}}\right)^{-1/\xi^{(m)}-1}$$

is the likelihood function. In the proposed FL-based GPD model regression, all sensors and the controller collaborate to learn the GPD model without sharing their own data set $\mathcal{Q}_k^{(m)}, \forall\, k \in \mathcal{K}$. That is, sensor k locally minimizes the KL divergence (28) and iteratively runs the gradient decent algorithm with its $\mathcal{Q}_k^{(m)}$ to train a local GPD model. Due to the unavailability of the closed-form solution to problem (28), we resort to the iterative gradient decent approach [19] for sensor k, i.e.,

$$\theta_k^{n+1} = \theta_k^n - \delta_{\theta,k}^n \nabla G(\theta_k^n|\mathcal{Q}_k),\ n = 0, 1, 2, \cdots, \tag{29}$$

Procedure 1 Lyapunov-Based Iterative Transmission Optimization Scheme (Lya-ITOS)

Input: $C_g, M, W_{obs}, \mathcal{K}, f_m, f_{es}, \epsilon_{es}, f_{ea}, \epsilon_{ea}, p_{max}, B, N_0, V, \rho$.
// W_{obs} is the time window for each iteration
Output: $O_k(\cdot)$, $\forall k \in \mathcal{K}$.
Initialize: $\tau_k(0|C_g) = 0, a_k(0|C_g) = 0, b_k(1|C_g) = 0, q_k(1|C_g) = 0, \Gamma_k(0|C_g) = 0, \Lambda_k(0|C_g) = 0$, $\forall k \in \mathcal{K}, \theta^{(0)} = \{10^{-2}, 10^{-4}\}$, $(p_k^{(0)})^* = 0$.
// the conditional term $(\cdot|C_g)$ is omitted in the following pseudo codes
for $m = 0, 1, \cdots, M-1$ **do**
  for $\forall k \in \mathcal{K}$ **do**
    Sample the data with C_g and record $h_k(i|C_g)$ and $\tau_k(i)$.
    for $i = 1, 2, \cdots,$: $\forall \tau_k(i) \in W_{obs}^{(m)}$ **do** *// Start of L-TEO*
      Form $\chi_k'(i), \chi_k''(i)$ in (15) and solve $p_k^{(m)})^*(i)$ by CCP (16),
      Transmit the i-th sampled data with $p_{EXT,k}^{(m)}(i)$ by (26) or $p_{APP,k}^{(m)}(i)$ by (27),
      Update $t_k(i), q_k(i), a_k(i), f_k(i)$ by (1), (2), (3), (4),
      $\Gamma_k(i+1), \Lambda_k(i+1)$ by (12) and (13),
    end for *// End of L-TEO*
    Consolidate $\mathcal{Q}_k^{(m)}$ and train $\hat{\theta}_k^{(m)}$ by (29), and (30),
    // Start of GPD-TEE
    Upload $\hat{\theta}_k^{(m)}$ to the controller and get $\theta^{(m)}$ by (31),
    Calculate $(\Delta p_k^{(m)})^*$ with $\theta^{(m)}$ by solving (24) with (25),
    // End of GPD-TEE
  end for
end for
for $\forall k \in \mathcal{K}$ **do**
  Calculate and return $O_k(\cdot) = Cost_k(C_g)$ by (32)-(36).
  // Preparing for Bay-SCOS
end for

in which n is the iteration index. Here, $\delta_{\theta,k}^n$ is the flexible step size varying with iterations [38], and

$$\begin{aligned} \nabla G(\theta|\mathcal{Q}) &= \begin{bmatrix} \dfrac{\partial G(\theta|\mathcal{Q})}{\partial \sigma} \\ \dfrac{\partial G(\theta|\mathcal{Q})}{\partial \xi} \end{bmatrix} \\ &= \begin{bmatrix} \displaystyle\sum_{\hat{f}\in\mathcal{Q}} \frac{\sigma - \hat{f}}{\sigma(\sigma + \xi\hat{f})} \\ \displaystyle\sum_{\hat{f}\in\mathcal{Q}} \left[\frac{\hat{f}(1+\xi)}{\xi(\sigma+\xi\hat{f})} - \frac{1}{\xi^2}\ln\left(1 + \frac{\xi\hat{f}}{\sigma}\right)\right] \end{bmatrix}. \end{aligned} \tag{30}$$

For notational simplicity, we ignore superscript (m) in (29) and (30). When convergence is achieved, i.e., $|\theta_k^n - \theta_k^{n-1}| \to 0$, the learned GPD model of sensor k in the (m)-th iteration is set as $\hat{\theta}_k^{(m)} = \theta_k^n$. Next, sensor k uploads $\hat{\theta}_k^{(m)}$ and the value of $|\mathcal{Q}_k^{(m)}|$ to the controller. Based on the uploaded information, the controller calculates the global GPD model as

$$\theta^{(m)} = \frac{1}{|\mathcal{Q}^{(m)}|}\sum_{k\in\mathcal{K}} |\mathcal{Q}_k^{(m)}|\hat{\theta}_k^{(m)}, \tag{31}$$

which is then fed back to all sensors for GPD-TEE as mentioned in Section III-A2. Moreover, the initial set θ_k^0 in (29) for every sensor k's next $(m+1)$-th *FL-based GPD Model Regression* is given from $\theta^{(m)}$ in (31) as well. The steps of Lya-ITOS are outlined in Procedure 1.

B. Bayesian Optimization-Based Sampling Criterion Optimization Scheme (Bay-SCOS)

After the total M iterations of Lya-ITOS are finished with the given C_g, we verify the corresponding utility for problem (8) to forage out another unexplored potential value of C_g.

Note that the values of the virtual queues in Lyapunov optimization reflect the satisfaction level of the corresponding constraints. Thus, we incorporate the optimal result of (8a) and the virtual queues' average values obtained in Lya-ITOS through all the M iterations as a cost function to measure the system performance under a given C_g. To this end, the cost function of sensor $k \in \mathcal{K}$ is coined as

$$Cost_k(C_g) = \alpha C_g + \overline{E}_k^{(ERM)}(C_g) + \frac{1}{V}\left[\overline{\Gamma}_k(C_g) + \overline{\Lambda}_k(C_g) + \overline{\Upsilon}_k(C_g)\right], \quad (32)$$

where

$$\overline{E}_k^{(ERM)}(C_g) = \lim_{I\to\infty} \frac{1}{\rho} \ln\left(\frac{1}{I}\sum_{i=1}^{I} \exp\left(\rho E_k^*(i|C_g)\right)\right), \quad (33)$$

$$\overline{\Gamma}_k(C_g) = \lim_{I\to\infty} \frac{1}{I}\sum_{i=1}^{I} \Gamma_k\big(i\big|C_g\big), \quad (34)$$

$$\overline{\Lambda}_k(C_g) = \lim_{I\to\infty} \frac{1}{I}\sum_{i=1}^{I} \Lambda_k\big(i\big|C_g\big), \quad (35)$$

$$\overline{\Upsilon}_k(C_g) = \lim_{I\to\infty} \frac{1}{I}\sum_{i=1}^{I} \Upsilon_k\big(i\big|C_g\big), \quad (36)$$

and the virtual queue $\Upsilon_k\big(i\big|C_g\big)$ under a given C_g with the queue evolution

$$\Upsilon_k(i+1) = [\Upsilon_k(i) + (\mathbb{1}_{\{f_k(i)>f_{es}\}} - \epsilon_{ea}) f_k(i)]^+,$$

$\forall\, i \in \mathbb{Z}^+$, $\forall\, k \in \mathcal{K}$, is for the extreme staleness exccedance constraint (7). To estimate the cost of the unexplored value of C_g, we adopt BO which combines Gaussian process regression (GPR) for model training and efficient global optimization (EGO) [39]. Let us elaborate on Bay-SCOS as follows.

1) Gaussian Process Regression (GPR) for Model Training: Assuming the system has explored S cost values with the corresponding values of C_g, we denote the well-explored sampling frequency set as

$$\mathcal{C}_g(S) = [C_g(1), C_g(2), \cdots, C_g(S)]^T \in \mathbb{R}^{S\times 1}.$$

With the sensor k's corresponding local cost $O_k(s) = Cost_k(C_g(s))$, $s = 1, 2, \cdots, S$, we denote the local cost vector set as $\mathcal{O}_k(S) = [O_k(1), O_k(2), \cdots, O_k(S)]^T \in \mathbb{R}^{S\times 1}$. The ultimate goal is to find a zero-mean noise-free S-variable global normal distribution function which has the closest KL divergence to

$$\mathcal{O}(S) \sim \mathcal{N}(0, \Pi(\vartheta(S))) \quad (37)$$

with the global cost vector

$$\mathcal{O}(S) = \frac{1}{|\mathcal{K}|}\sum_{k\in\mathcal{K}} \mathcal{O}_k(S) = [O(1), O(2), \cdots, O(S)]^T \in \mathbb{R}^{S\times 1}. \quad (38)$$

In (37), $\Pi(\vartheta(S)) \in \mathbb{R}^{S\times S}$ is the global covariance matrix with the global hyperparameter set $\vartheta(S)$ of the element function. Here, we utilize squared exponential covariance as the element function to emulate the trend of the cost value with respect to C_g. The (i,j)-th element in $\Pi(\vartheta(S))$ is

$$\pi(i,j) = \eta^2 \exp\left(\frac{-(C_g(i) - C_g(j))^2}{2\nu^2}\right),\ \forall\, i,j = 1, 2, \cdots, S, \quad (39)$$

with the hyperparameter set $\vartheta(S) = (\eta(S), \nu(S))$. We abbreviate $\Pi(\vartheta(S))$ to Π^S in the rest of content for notational simplicity. To obtain the optimal hyperparameter set, the objective is

$$\hat{\vartheta} = \arg\min_{\vartheta\in\mathbb{R}^2} \mathcal{B}(\vartheta|\mathcal{O}(S)), \quad (40)$$

where

$$\mathcal{B}(\vartheta|\mathcal{O}(S)) = -\ln \mathcal{N}(\mathcal{O}(S)|0, \Pi^S) = \tfrac{1}{2}[(\mathcal{O}(S))^T(\Pi^S)^{-1}\mathcal{O}(S) + \ln(\det(\Pi^S)) + S\ln(2\pi)].$$

In the proposed FL-based GPR, sensor k trains the local model with ϑ_k by

$$\hat{\vartheta_k} = \arg\min_{\forall\vartheta_k\in\mathbb{R}^2} \mathcal{B}(\vartheta_k|\mathcal{O}_k(S)) \quad (41)$$

and the iterative gradient decent [19]

$$\vartheta_k^{n+1} = \vartheta_k^n - \delta_{\vartheta,k}^n \nabla\mathcal{B}(\vartheta_k^n|\mathcal{O}_k(S)),\ n = 0, 1, 2, \cdots. \quad (42)$$

Here, $\vartheta_k^0 = \hat{\vartheta}(S-1)$ is the global hyperparameter set leveraged by the controller in the previous operation (i.e., when only having $(S-1)$ costs of the corresponding explored C_g-value). Additionally, $\delta_{\vartheta,k}^n$ is the flexible step size of sensor k [38], and

$$\nabla\mathcal{B}(\vartheta|\mathcal{O}(S)) = \tfrac{1}{2}\left[tr\big((\Pi^S)^{-1}\tfrac{\partial\Pi^S}{\partial\vartheta}\big) - \mathcal{O}^T(S)(\Pi^S)^{-1}\tfrac{\partial\Pi^S}{\partial\vartheta}(\Pi^S)^{-1}\mathcal{O}(S)\right]$$

is the derivative of the negative log S-variable normal distribution model, in which $\frac{\partial\Pi^S}{\partial\vartheta}$ is the element-wise partial derivative of the covariance matrix

$$\frac{\partial\pi(i,j)}{\partial\vartheta} = \begin{bmatrix} \dfrac{\partial\pi(i,j)}{\partial\eta} \\ \dfrac{\partial\pi(i,j)}{\partial\nu} \end{bmatrix} = \begin{bmatrix} 2\eta\exp\big(\frac{-(C_g(i)-C_g(j))^2}{2\nu^2}\big) \\ \dfrac{\eta^2(C_g(i)-C_g(j))^2}{\nu^3}\exp\big(\frac{-(C_g(i)-C_g(j))^2}{2\nu^2}\big) \end{bmatrix}, \quad (43)$$

$\forall\, i,j = 1, 2, \cdots, S$. Sensor k harvests the local optimal hyperparameter set as $\hat{\vartheta}_k(S) = \vartheta_k^n$ when $|\vartheta_k^n - \vartheta_k^{n-1}| \to 0$, and reports $\hat{\vartheta}_k(S)$ to the controller. Then, the controller obtains the global optimal hyperparameter set by leveraging

$$\hat{\vartheta}(S) = \frac{1}{|\mathcal{K}|}\sum_{k\in\mathcal{K}} \hat{\vartheta}_k(S). \quad (44)$$

2) Efficient Global Optimization (EGO)-Based Sampling: With $\hat{\vartheta}$, we form the global posterior noise-free S-variable normal distribution of the u-th global cost (the corresponding $C_g(u)$ can be one of the well-explored one or any other unexplored one) as

$$O(u) = Cost(C_g(u)) \sim \mathcal{N}\big(\mu(C_g(u)|\hat{\vartheta}), \varpi(C_g(u)|\hat{\vartheta})\big), \tag{45}$$

$\forall\, u \in \mathbb{Z}^+$. For notational simplicity, the term $\hat{\vartheta}$ is ignored, and $C_g(u)$ is abbreviated as u in the remainder of Section III-B2. In (45), the mean of $Cost(C_g(u))$ is

$$\mu(u) = \mathbb{E}[Cost(C_g(u))] = [\Xi^S(u)]^T(\Pi^S)^{-1}\mathcal{O}^S \in \mathbb{R},$$

and the variance of $Cost(C_g(u))$ is

$$\begin{aligned}\varpi(u) &= Var[Cost(C_g(u))] \\ &= \hat{\eta}^2 - [\Xi^S(u)]^T(\Pi^S)^{-1}\Xi^S(u) \in \mathbb{R}^+,\end{aligned}$$

where $\Xi^S(u) = [\pi(u,1), \cdots, \pi(u,S)]^T \in \mathbb{R}^{S\times 1}$ is the covariance vector between the u-th global cost and well-explored global cost set $\mathcal{O}(S)$ as (38).

With EGO [39], the central processor estimates the next potential value of C_g with the improvement value, defined as $IM(O(u)) = [O_{min} - O(u)]^+$, where $O_{min} = \min\{\mathcal{O}(S)\}$ is the minimum well-explored global cost. To figure out the expectation of the improvement, we have $\mathbb{E}[IM(O(u))] = \mathbb{E}\big[O_{min} - O(u)]^+\big]$, which can be expressed in a closed form by applying integration by parts [39], and obtain

$$\mathbb{E}[IM(O(u))] = \zeta(u)\Phi\left(\frac{\zeta(u)}{\sqrt{\varpi(u)}}\right) + \sqrt{\varpi(u)}\phi\left(\frac{\zeta(u)}{\sqrt{\varpi(u)}}\right). \tag{46}$$

Here, $\zeta(u) = O_{min} - \mu(u)$. $\phi(\cdot)$ and $\Phi(\cdot)$ represent the probability density function and CDF. Hence, we predict next potential sampling as per

$$u' = \arg\max_{\forall u \in \mathbb{Z}^+} \mathbb{E}[IM(O(u))]. \tag{47}$$

Once the controller finds an unexplored potential C_g, it will announce to all sensors and start a new exploration. The well-explored C_g set will extend in the exploration period, e.g., from S to $S+1$, after the sensors report the local cost vector $\mathcal{O}_k(S+1)$, $\forall k \in \mathcal{K}$, to the controller in order to obtain the global cost vector $\mathcal{O}(S+1)$. The controller will cease the exploration until the latest most potential C_g duplicates the one in the well-explored set. Then, the controller finally selects the C_g within the well-explored set which results in the minimum cost as the optimal solution to (8). The steps of Bay-SCOS and FLTS-SETOS are outlined as Procedure 2 and Algorithm 1, respectively.

The operation of FLTS-SETOS is summarised below. As shown in Algorithm 1, FLTS-SETOS firstly sets State as *"true"* (which means such C_g has potential to improve the system performance) for the initial C_g. With the initial C_g, FLTS-SETOS performs Lya-ITOS to optimize the long-term ERM data transmission energy consumption, i.e., the optimal solution of (9), and forms the cost value of each sensor, i.e., (32), with virtual queues. Furthermore, collecting the global cost value(s) with the corresponding C_g(s), FLTS-SETOS runs Bay-SCOS to check if there is another potential C_g. As depicted in Line 7 of Algorithm 1, Bay-SCOS returns *"true"* when a new C_g is explored, and Lya-ITOS will be executed accordingly. On the other hand, if there is no explored C_g, Bay-SCOS will return *"false"* and the optimal C_g by searching the historical cost results. To this end, FLTS-SETOS retrieves the corresponding result of Lya-ITOS with the optimal C_g as the final solution.

Procedure 2 Bayesian-Based Sampling Optimization Scheme (Bay-SCOS)

Input: $S, \mathcal{C}_g(S), \mathcal{O}_k(S)$, $\forall k \in \mathcal{K}$. *// W_{obs} is the time window for each iteration*
Output: {*"true"*, $C_g(S+1)$} *or* {*"false"*, C_s^*}.
1: **for** $\forall k \in \mathcal{K}$ **do**
2: Calculate and return $\hat{\vartheta_k}$ with $\mathcal{O}_k(S)$ by (41) and (42), *// GPR part*
3: **end for**
4: Aggregate $\mathcal{O}(S)$ with $\mathcal{O}_k(S)$, $\forall k \in \mathcal{K}$ by (38), and $\hat{\vartheta}$ with $\hat{\vartheta_k}$, $\forall k \in \mathcal{K}$ by (44), *// start of GEO*
5: **for** $u = 1, 2, \cdots \in \mathbb{Z}^+$ **do** *// check within the exploration region*
6: Calculate the distribution of $O(u)$ by (45), and $\mathbb{E}[IM(O(u))]$ by
7: (46),
8: **end for**
9: Obtain u' by (47),
10: **if** $C_g(u') \notin \mathcal{C}(S)$ **then**
11: $C_g(S+1) \leftarrow C_g(u')$, return {*"true"*, $C_g(S+1)$},
12: **else**
13: $C_s^* : \mathcal{C}_g(S) \leftarrow \arg\min_{\forall s \in S} \mathcal{O}(S)$, return {*"false"*, C_s^*}.
14: **end if** *// End of GEO*

Algorithm 1 FL-Based Two-Stage Sampling-Frequency and Energy Trade-Off Scheme (FLTS-SETOS)

Input: $M, W_{obs}, \mathcal{K}, f_m, f_{es}, \epsilon_{es}, f_{ea}, \epsilon_{ea}, p_{max}, B, N_0, V, \rho$.
Output: $C_s^*, E_k(i|C_s^*), \forall k \in \mathcal{K}, \forall i$,
Initialize: $S = 0, C_g(1), \mathcal{C}_g(0) = \{\}, \hat{\vartheta}^{(0)} = \{1, 1\}, \mathcal{O}(0) = \{\}, \mathcal{O}_k(0) = \{\}, \forall k \in \mathcal{K}$, State ="*true*",
1: **while** State ="*true*" **do**
2: $S = S+1$, $\mathcal{C}_g(S) = \{\mathcal{C}_g(S-1) \quad C_g(S)\}$,
3: $[O_k(S), \forall k \in \mathcal{K}] =$ Lya-ITOS$\{C_g(S), M, W_{obs}, \ \cdots$
$\mathcal{K}, f_m, f_{es}, \epsilon_{es}, f_{ea}, \epsilon_{ea}, p_{max}, B, N_0, V, \rho\}$,
4: **for** $k \in \mathcal{K}$ **do**
5: $\mathcal{O}_k(S) = \{\mathcal{O}_k(S-1) \quad O_k(S)\}$,
6: **end for**
7: [{*"true"*, $C_g(S+1)$}/{*"false"*, C_s^*}] = $\cdots$
Bay-SCOS$\{S, \mathcal{C}_g(S), \mathcal{O}_k(S), \forall k \in \mathcal{K}\}$,
8: **end while**
9: Return the C_s^* corresponding $E_k(i|C_s^*), \forall k \in \mathcal{K}, \forall i$ from Bay-SCOS.

IV. Numerical Results

We consider a 100-meter radius circular factory field. The controller is located in the center of the field, which is uniformly surrounded by $|\mathcal{K}| = 15$ sensors. Since smart grid, one promising application of 5G networks [40], requires timely and stringent status monitoring, we consider the voltage amplitude of the alternating current [41]. Thus, for each sensor $k \in \mathcal{K}$, the continuous monitoring curve of the environmental changes $H_k(t)$ follows the same distribution as per

$$H_k(t) = A_{mp}\sin(t \cdot 2\pi + \theta_k^{(sft)}) + n_k^{(rp)}(t), \ \forall\, t \in \mathbb{R}^+, \tag{48}$$

where A_{mp} is the amplitude of the change, $\theta_k^{(sft)} \sim \mathcal{U}(0, 2\pi)$ is the phase shift in the beginning, and $n_k^{(rp)}(t)$ is the 20 dB standard deviation of environmental random perturbation. The considered path loss model between the controller and each sensor $k \in \mathcal{K}$ is the 3GPP TR 38.901 in-field loss [42] function

$$PL_k = 31.84 + 21.5 \cdot \log_{10}(d_k) + 19 \cdot \log_{10}(f_c) + n_k^{(s)}.$$

This article has been accepted for publication in IEEE Transactions on Communications. This is the author's version which has not been fully edited and content may change prior to final publication. Citation information: DOI 10.1109/TCOMM.2022.3216353

A_{mp}	10	B	30k Hz	N_0	-174 dBm
κ_{cpu}	10^{-27}	D_{raw}	100 byte	D_{mdl}	240 byte
f_{es}	$2 \cdot 10^{-2}$	ϵ_{es}	10^{-3}	f_{ea}	10^{-2}
F_{raw}	10^3 cycle/s	T_{prs}	10 ms	S_b	3
ϵ_{ea}	0.5	ρ	5	D_{env}	$3 \cdot 10^3$ byte
$\mathcal{U}$	$2 : 10^{-2} : 2.8$	M	600	W_{obs}	1 sec
p_{max}	20 dBm	V	1	d_k	$(0, 100]$ m
f_c [42]	3.5 GHz	n_{cpu}^{sen}	1	n_{cpu}^{ctr}	8

Table I: Simulation Parameters

Note that $n_k^{(s)}$ is a 4 dB-fading-effect of shadowing. Furthermore, the channel gain in (1) is expressed as

$$h_k(i|C_g) = 10^{(-PL_k/10)} \cdot \psi,$$

in which ψ denotes the Rayleigh fading with unit variance.

In the analysis of the energy-saving benefits, we consider the same scheme as FLTS-SETOS. However, in the CL-based approach, all the raw data are consolidated centrally for model training. To verify the model-training energy consumption, we adopt the computational energy function [26] as per

$$E_{com}(L_{raw}) = \frac{\kappa_{cpu}[F_{raw}L_{raw}]^3}{(n_{cpu}T_{prs})^2},$$

and transmission energy for the raw data exchanging in CL or local model exchanging in FL between the sensor $k \in \mathcal{K}$ and the controller is formed as

$$E_{trn}^k(\tilde{L}) = \frac{T_{prs}N_0B}{\tilde{h}_k}\left[\exp\left(\frac{(\ln 2)\tilde{L}}{T_{prs}B}\right) - 1\right],$$

where κ_{cpu} is CPU effective switched capacitance. Additionally, F_{raw} in cycle/bit is the required computation frequency [43], and n_{cpu} is the number of the working CPU which can be n_{cpu}^{sen} or n_{cpu}^{ctr} for the sensors or the controller. T_{prs} is the processing time for either computation or transmission in model training. We consider the statistical-average in-field path loss $\tilde{h}_k$ in between. Note that the transmit power $p_{trn}^k(\tilde{L}) = \frac{N_0B}{\tilde{h}_k}\left[\exp\left(\frac{(\ln 2)\tilde{L}}{T_{prs}B}\right) - 1\right]$ in $E_{trn}^k(\tilde{L})$ is different from $p_k(i|C_g)$ in (8) without the power budget constraint. Moreover, $\tilde{L}$ is the size in byte which can be L_{raw} for the raw data or D_{mdl} for the local model, respectively. $L_{raw} = N_{raw}D_{raw}$ considers the number of raw data N_{raw} with size D_{raw}. In addition, since the model is aggregated by averaging, such computation energy is relatively tiny compared with model training [43] and thus is ignored here. In Section IV-A, we fix the trade-off parameter $\alpha = 10$ and discuss the impacts of varying α in Section IV-B. The rest of the parameter settings are listed in Table I. To verify FLTS-SETOS, we decompose it and check the results of the sub-schemes, Lya-ITOS and Bay-SCOS, individually.

A. Performance Evaluation of FL-Based Lya-ITOS

1) GPD Model Training in GPD-TEE: To concentrate on the GPD model training performance in GPD-TEE without any effects from L-TEO, we verify the regression of the first Lya-ITOS iteration, i.e., $m = 1$ and $(\Delta p_k^{(0)})^* = 0$, as an original result in Fig. 3. Under $C_g = 2.1$, Fig. 3a illustrates the CCDF results with the GPD regression parameters obtained by (28) and (29) from CL and GPD-TEE. While directly training the global raw data, the results of CL are more close to the empirical one, where the results of GPD-TEE more underestimate the extreme staleness distribution. To quantify the regression accuracy, we take the root-mean-square error (RMSE) of the CCDFs between the schemes and the empirical one. In Fig. 3a, the RMSE of CL is 0.0253, which is 20.9% less than GPD-TEE's 0.0320.

Fig. 3b presents the RMSE results. The results of CL are relatively stable under all values of C_g and are better than GPD-TEE. When C_g grows, the time difference between two successive sampled data becomes greater, and the extreme staleness happens rarely, which makes each sensor lack training data and causes severely training inaccuracy in GPD-TEE. Such drawback is mitigated in the CL-based scheme since the controller trains the data after gathering all the data from the sensors.

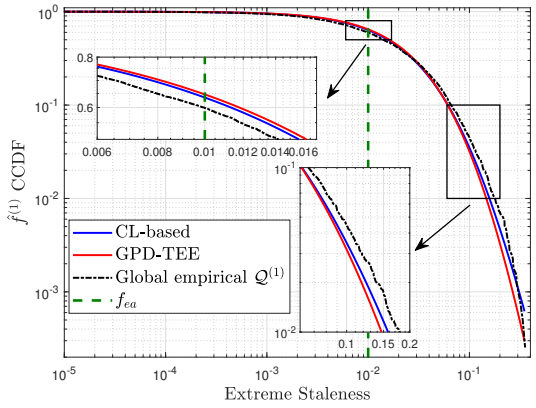

(a) $\hat{f}^{(1)}$ CCDF profile under $C_g = 2.1$

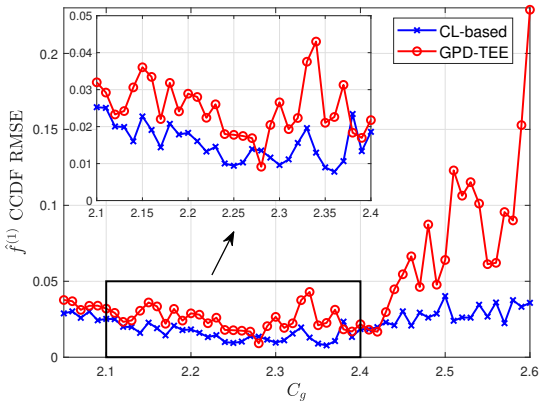

(b) The RMSE difference

Figure 3: The GPD regression results

The obtained increased power $(\Delta p_k^{(1)})^*$ in the first iteration $(m = 1)$ is given in Fig. 4. As mentioned before, GPD-TEE underestimates the CCDF more. Hence, the increased power obtained by GPD-TEE is less than the power in the CL-based scheme. Note that even GPD-TEE's RMSE gains more dramatically than the CL-based scheme as shown Fig. 3b with the increase of C_g, the gap of $(\Delta p_k^{(1)})^*$ does not increase significantly. That is because although the regression result of GPD-TEE in large C_g deviates more, the obtained result

This article has been accepted for publication in IEEE Transactions on Communications. This is the author's version which has not been fully edited and content may change prior to final publication. Citation information: DOI 10.1109/TCOMM.2022.3216353

of extreme staleness exceedances (7) for satisfaction is still similar.

Fig. 5 shows the GPD model-training energy consumption $E^{GPD}_{learn}(C_g)$ for completing the schemes, e.g., after performing M-iteration. While jointly considering computation and transmission energy (denoted by E_{com} and E_{trn}), we derive $E^{GPD}_{learn}(C_g)$ as

GPD-TEE:

$$E^{GPD}_{learn}(C_g) = \sum_{m=1}^{M} \Bigg[\sum_{\forall k \in \mathcal{K}} \Big[E_{com}(|\mathcal{Q}_k^{(m)}|D_{raw}) + 2 \cdot E^k_{trn}(D_{mdl}) \Big] \mathbb{1}_{\{|\mathcal{Q}_k^{(m)}| \geq S_b\}} \Bigg] \Big|_{(C_g)},$$

CL-based:

$$E^{GPD}_{learn}(C_g) = \sum_{m=1}^{M} \Bigg[\sum_{\forall k \in \mathcal{K}} E^k_{trn}(|\mathcal{Q}_k^{(m)}|D_{raw}) + E_{com}(|\mathcal{Q}^{(m)}|D_{raw}) \mathbb{1}_{\{|\mathcal{Q}^{(m)}| \geq S_b\}} \Bigg] \Big|_{(C_g)},$$

in which $|\mathcal{Q}^{(m)}| = \sum_{\forall k \in \mathcal{K}} |\mathcal{Q}_k^{(m)}|$, and S_b is the batch size, i.e., the size $|\mathcal{Q}_k|$ in (29). In the GPD model-training energy consumption function, the model transmission energy $E_{trn}(D_{mdl})$ is doubled for uploading the local model and returning the aggregated one. In Fig. 5, the training energy consumption of GPD-TEE is always smaller than that of the CL-based scheme.

When the value of C_g is small, the sensors sample the environment more frequently and accumulate considerable data to transmit, resulting in an increased occurrence rate of extreme staleness. In the CL-based scheme, the sensors have to consume lots of energy to deliver the extreme staleness raw data to the controller. However, in GPD-TEE, since the sensors only deliver the model with fixed size, the transmission energy for local-model updating does not increase with the high occurrence rate of extreme staleness. Additionally, in the large C_g cases, e.g., under 2.32, the extreme staleness happens too rarely for the sensors to fill up the local batch size S_b in every iteration, which significantly reduces the local computation energy consumption in GPD-TEE but occurs great deviation as mentioned in Fig. 3b. Nonetheless, such deviation does not degrade the system performance much as mentioned previously. In the case of $C_g = 2.1$, the increased power $(\Delta p_k^{(1)})^*$ obtained by GPD-TEE is 8.62% less than the CL-based scheme as shown in Fig. 4, but consumes only 0.157 Joule, which is only 30.858% energy of the CL-based scheme's 0.509 Joule for GPD model training as shown in Fig. 5.

2) Proposed APP and EXT in GPD-TEE: The proposed cost function and the ERM energy consumption after completing M iterations are shown in Fig. 6, and the corresponding global means of the virtual queues are plotted in Fig. 7. Therein, we elaborate on the combination of the proposed GPD-TEE and CL with APP and EXT, individually. Moreover, we take W/O as the scheme without considering extreme staleness exceedance constraints (7) as the worst-case baseline. Recap that the proposed cost function is composed with the

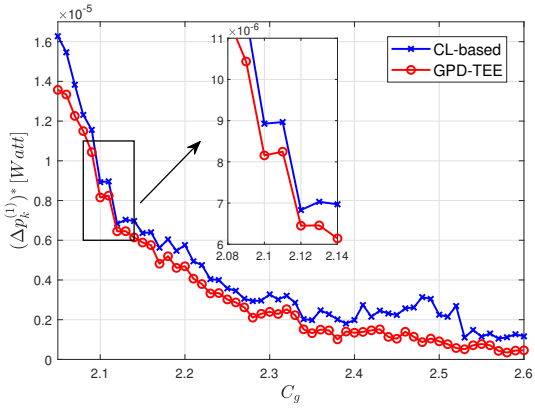

Figure 4: The derived increased power

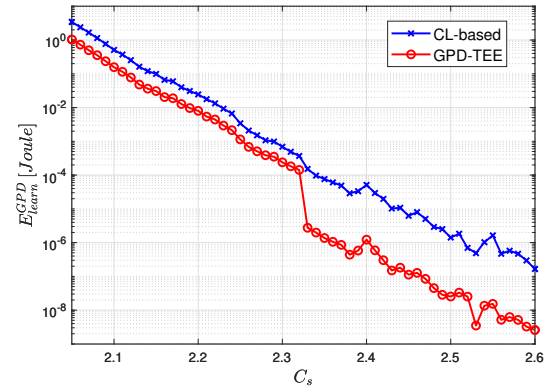

Figure 5: The GPD regression energy

mean of ERM energy consumption and virtual queues. In Fig. 6a, under EXT, the curves of CL and GPD-TEE almost overlap with each other since EXT only adjusts the transmit power of the extreme staleness which is yet in the high power level and capped by the power budget p_{max}, making the performance of EXT schemes limited and similar. In the cases of small C_g, the EXT schemes have limited improvement to W/O due to the power budget restriction. On the contrary, APP schemes decrease the system cost dramatically since the adjusted power is apportioned to all data transmissions. The extreme staleness is mitigated in every data transmission, which may not be restricted by the power budget as severely as the EXT schemes. This shows that APP outperforms EXT in the worst-case scenario, i.e., Corollary 1 in Section III-A2. Furthermore, the APP scheme with CL outperforms the APP scheme with GPD-TEE due to the GPD model training accuracy as mentioned before. Fig. 6b reflects the severe restriction of the power budget for the EXT schemes in the cases of small C_g. The APP schemes consume more energy to meet the constraints (5), (6), and (7), and lower down the volumes of the corresponding virtual queues (34), (35), and (36) as shown in Figs. 7a, 7b, and 7c. Even though the APP schemes consume the most energy, the costs are reduced significantly in the cases of small C_g in Fig. 6a.

In Lyapunov optimization, the virtual queue value in the steady state depends on the numerology and satisfaction level of the corresponding constraints as mentioned in Section III-B.

This article has been accepted for publication in IEEE Transactions on Communications. This is the author's version which has not been fully edited and content may change prior to final publication. Citation information: DOI 10.1109/TCOMM.2022.3216353

That is, the number will be higher/lower if the constraint is under/over-satisfied. The APP schemes' virtual queue values in Fig. 7 are greater than those of the EXT schemes after a certain values of C_g, e.g., after 2.22 in Fig. 7b. The reason is that the APP schemes are more resilient for the transmit power adjustment for just meeting the corresponding requirements, rather than over-satisfying the constraints as EXT schemes. This also explains that the APP schemes' ERM energy consumption in Fig. 6b is less than the EXT schemes', but the system cost in Fig. 6a gets higher after $C_g = 2.22$.

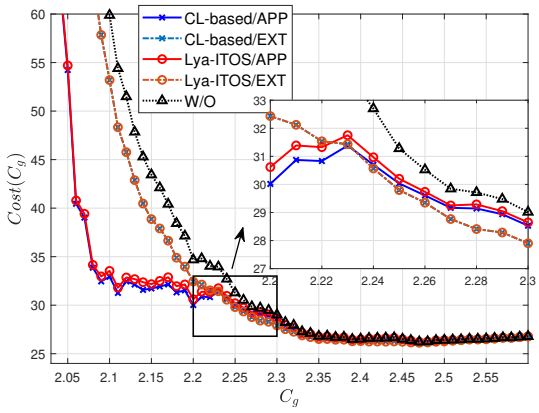

(a) The system cost (32)

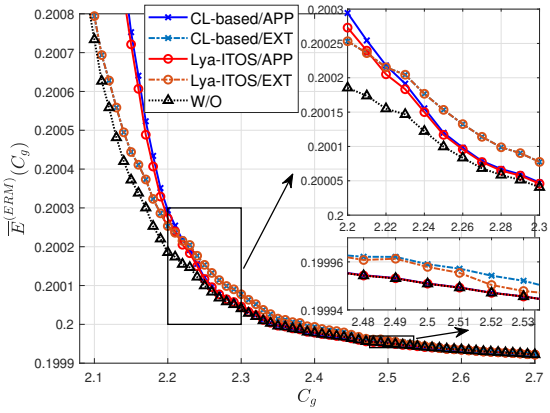

(b) The system ERM energy consumption (33)

Figure 6: Performance of the proposed APP and EXT

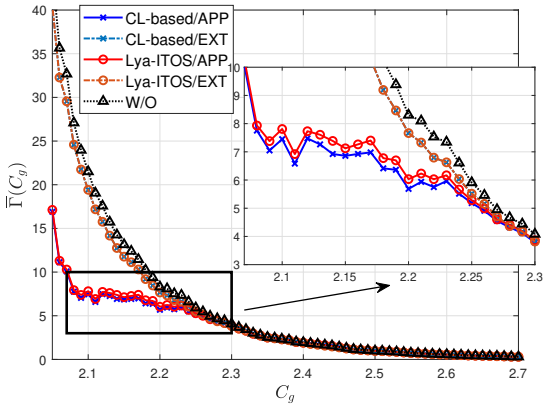

(a) Virtual queue (34)

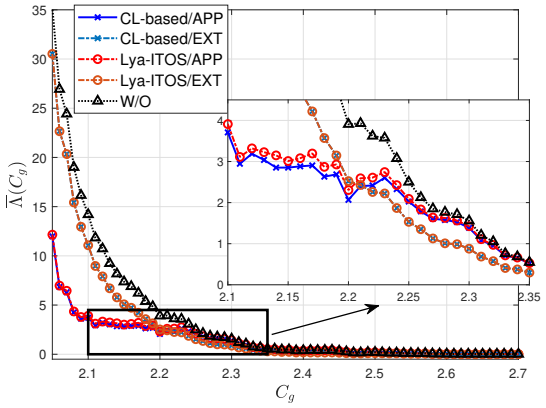

(b) Virtual queue (35)

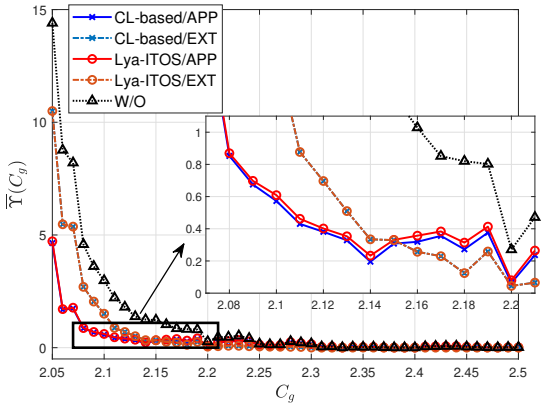

(c) Virtual queue (36)

Figure 7: System virtual queues

B. Performance Evaluation of FL-Based Bay-SCOS

We compare the Bay-SCOS estimation with the CL paradigm which follows up with the APP scheme and takes the corresponding system cost results as the ground truth in Fig. 8 under $\alpha = 10$. The APP-based GPD-TEE's system cost ground truth is similar but slightly higher than that of the CL one, due to the GPD model regression deviation as mentioned before. While randomly picking the initial C_g as 2.33, Figs. 8a and 8c show the results after having three well-explored values of C_g. As the figures present, the CL-based scheme possesses a higher variance around the global minimum point, making it easier to hit the bull's eye. In addition, Figs. 8b and 8d show the final results after each scheme finishes exploration. The CL-based scheme hits the global minimum point $Cost(2.47) = 26.207$ after exploring eight values of C_g. However, Bay-SCOS misses the global optimal point $Cost(2.47) = 26.217$ and stops at $Cost(2.48) = 26.241$ as the estimated minimum after experiencing nine-point C_g exploration. The estimated minimum cost is 0.092% more than the global one. In addition, APP-based GPD-TEE's global minimum cost is 0.038% more than that of the CL-based scheme. In summary, the minimum cost estimation of Bay-SCOS is $Cost(2.48) = 26.241$, which is only 0.13% higher than the CL-based scheme's $Cost(2.47) = 26.207$.

Fig. 9 shows the Bay-SCOS results under $\alpha = 5$ and 50. In Fig. 9a, Bay-SCOS takes the $Cost(2.55) = 13.783$ as

This article has been accepted for publication in IEEE Transactions on Communications. This is the author's version which has not been fully edited and content may change prior to final publication. Citation information: DOI 10.1109/TCOMM.2022.3216353

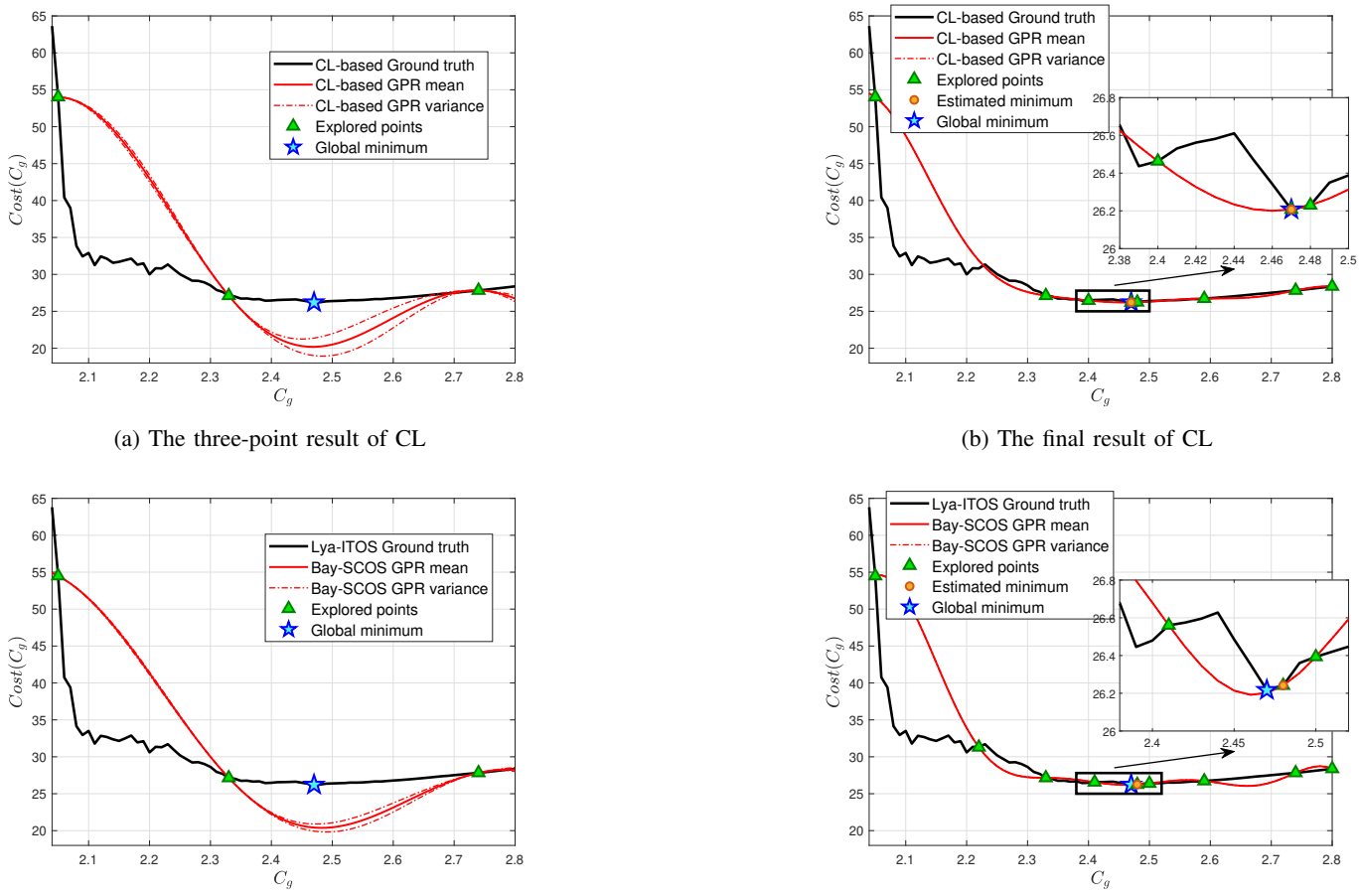

(a) The three-point result of CL

(b) The final result of CL

(c) The three-point result of Bay-SCOS

(d) The final result of Bay-SCOS

Figure 8: The BO performance under $\alpha = 10$

the estimated minimum point after eight-point exploration, which has 0.22% increase from the global minimum cost $Cost(2.58) = 13.754$. In Fig. 9b, Bay-SCOS finally hits the global minimum point $Cost(2.11) = 116.185$ after 14-point C_g exploration. Recap that α is the weight used to trade off the value of C_g and the long-term data transmission energy consumption. As the case of $\alpha = 5$ in Fig. 9a, C_g is less critical compared to the case of $\alpha = 10$. Hence, the global minimum system cost in $\alpha = 5$ appears at $C_g = 2.58$, which is greater than the global minimum point $C_g = 2.47$ in the case with $\alpha = 10$. On the contrary, for the case with relatively large $\alpha = 50$, the global minimum cost shows up at $C_g = 2.11$, which is relatively smaller.

Furthermore, for the energy consumption of BO under Bay-SCOS and the CL-scheme, we elaborate on the functions as follows. Regarding the common computation energy term, EGO searches the most potential C_g with (46) and (47) at the controller after the global GPR model is updated. We denote the EGO energy consumption as $E^{GEO}_{learn} = |\mathcal{U}|E_{com}(D_{mdl})$, where $\mathcal{U}$ is the set of the candidate values of C_g. In Section III-B1, the size of the GPR model variance matrix grows exponentially with S, i.e., the number of the well-explored value(s) of C_g. Thus, we derive the functions for each exploration as

Bay-SCOS:

$$E^{BO}_{learn}(S) = \sum_{\forall k \in \mathcal{K}} \Big[E_{com}(S^2 D_{raw}) + 2 \cdot E^{k}_{trn}(D_{mdl}) \Big] + E^{GEO}_{learn},$$

CL-based:

$$E^{BO}_{learn}(S) = \sum_{\forall k \in \mathcal{K}} E^{k}_{trn}(S D_{raw}) + E_{com}(|\mathcal{K}| S^2 D_{raw}) + E^{GEO}_{learn}.$$

Following up with the results in Figs. 8b and 8d, Bay-SCOS and the CL-based scheme explore nine and eight points to forage out the estimated optimal C_g, respectively. The exploration-step wide accumulative exploration energy consumption is illustrated in Fig. 10. After nine explorations, Bay-SCOS consumes 0.269 Joule, which is only 44.452% of the CL-scheme's energy consumption after eight exploration, i.e., 0.605 Joule.

C. The Trade-Off Between Training Performance and Energy Consumption

As mentioned in Section IV-B, given $\alpha = 10$, FLTS-SETOS's optimal system minimum cost is 26.241 under

This article has been accepted for publication in IEEE Transactions on Communications. This is the author's version which has not been fully edited and content may change prior to final publication. Citation information: DOI 10.1109/TCOMM.2022.3216353

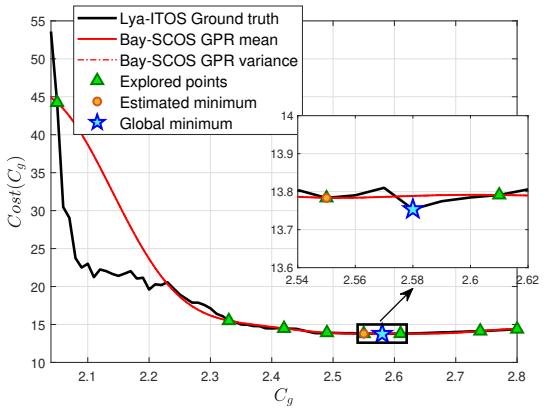

(a) $\alpha = 5$

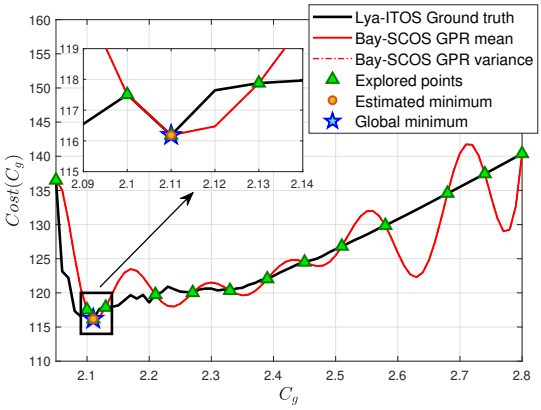

(b) $\alpha = 50$

Figure 9: Bay-SCOS performance

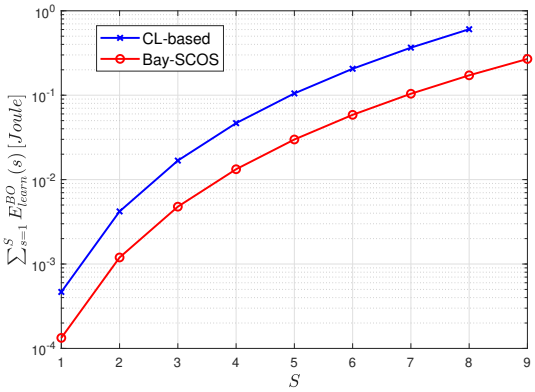

Figure 10: BO estimation energy consumption

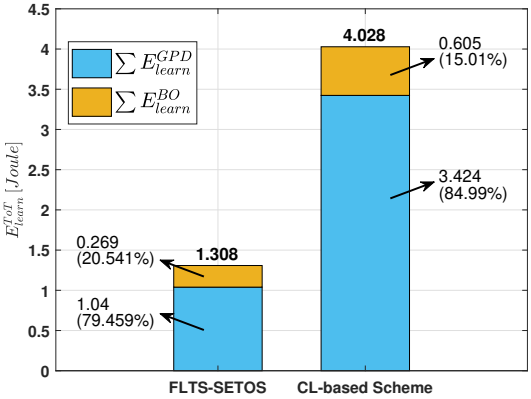

Figure 11: Breakdown of model training energy

$C_g = 2.48$ (although the ground truth is 26.217 under $C_g = 2.47$, the bias of C_g is 0.4%) which is 0.13% higher than the CL-based scheme's $Cost(2.47) = 26.207$. As shown in Fig. 6b, the long-term ERM sampled data transmission energy $\overline{E}^{(ERM)}(C_g)$ under the individual optimal C_g (2.48 in FLTS-SETOS and 2.47 in the CL-based scheme) are almost the same, while FLTS-SETOS consumes 9.936×10^{-5} additional to the CL-based scheme. Hence, we further compare the average transmission energy. For the optimal long-term global-average sampled data transmission energy $\overline{E}(C_g) = \lim_{I\to\infty} \frac{1}{I|\mathcal{K}|} \sum_{k\in\mathcal{K}} \left(\sum_{i=1}^{I} E_k^*(i|C_g) \right)$ for (8a), the proposed FLTS-SETOS transmits each sample data with 2.142×10^{-5} Joule in average, which is 6.3% additional to the CL-based's 2.015×10^{-5} Joule.

Finally, we count the total model training energy consumed by FLTS-SETOS and the CL-based scheme, respectively, which includes the two model-training energy consumptions

$$E_{learn}^{ToT}(\mathcal{C}_g(S)) = \sum_{C_g\in\mathcal{C}_g(S)} E_{learn}^{GPD}(C_g) + \sum_{s=1}^{S} E_{learn}^{BO}(s),$$

as presented in Fig. 11. Therein, FLTS-SETOS consumes 1.308 Joule for both GPD and BO training, which is only 30.790% of the energy taken by the CL-based scheme, 4.028 Joule. Therefore, the trade-off between the model training accuracy for boosting the system performance and the training energy consumption should be further considered.

V. Conclusions

This work studied a top-down IIoT network for environmental status monitoring, which jointly considers the data-sampling frequency and the long-term data transmission energy subject to the data staleness constraints. To seek the optimal solution, we proposed FL-based FLTS-SETOS composed of two schemes, Lya-ITOS and Bay-SCOS. Lya-ITOS finds the optimal solution under a given sampling criterion by iteratively performing L-TEO and GPD-TEE. L-TEO utilizes Lyapunov optimization to deal with the general staleness constraints to reach the long-term optimal transmission energy while GPD-TEE fulfills the extreme one. Subsequently, Bay-SCOS learns the most potential data-sampling criterion for the optimal data-sampling frequency to achieve the lowest value of the cost function. Note that we proposed the cost function in order to jointly examine the data-sampling criterion, the long-term data transmission energy, and the constraints' satisfaction condition. The simulation results articulate that the proposed FL-based scheme can save considerable computation energy and tolerate less performance loss. Compared with the CL-based scheme, numerical results show that the proposed FL-based FLTS-SETOS consumes only 31% energy for model training (GPD and GPR model regression) at the expense of a mere increase 6.3% in the global data transmission energy consumption (9.936×10^{-5} in entropic risk measure) under 0.4% bias from the global optimal data-sampling frequency and 0.13% increases of the system cost.

APPENDIX A
PROOF OF COROLLARY 1

With $a_k(i-1) - b_k(i) \geq 0, \forall i \in \mathbb{Z}^+, \forall k \in \mathcal{K}, w.p.\,1$, we index the data which experiences extreme staleness as n (theoretically $n \simeq 1/\epsilon_{es}$,) and express the AoI as

$$a_k(n) = \sum_{j=1}^{n} t_k(j) - \sum_{j=1}^{n} b_k(j).$$

Since the EXT scheme only powers up the data transmission for the extreme staleness, the AoI in EXT is expressed as

$$a_k^{(EXT)}(i) = \sum_{j=1}^{i-1} t_k(j|p_k(j)) + t_k(i|p_k(i) + \Delta p) - \sum_{j=1}^{i} b_k(j).$$

The APP scheme evenly distributes the power to each of the data transmission, which implies

$$a_k^{(APP)}(i) = \sum_{j=1}^{n} t_k(j|p_k(j) + \frac{1}{n}\Delta p) - \sum_{j=1}^{n} b_k(j).$$

In the following derivations, we abbreviate $t_k(x|p_k(x))$ to $t_k(x)$ for notational simplicity. Assuming $\Delta a_k(n) = a_k^{(APP)}(n) - a_k^{(EXT)}(n)$, we have (49). Here, we obtain the inequality (a) from the monotonically decreasing property of t_k with respect to p_k, i.e., (1). Since the extreme staleness cases happen when the queuing time q_k is large, the transmission time should be decreased as much as possible by increasing the transmit power. Hence, we have $p_k(n) \geq p_k(j), \forall j \neq n$, and the slop relation

$$\frac{n}{\Delta p}\left[t_k(n) - t_k\big(n|p_k(n) + \frac{1}{n}\Delta p\big)\right] \geq \frac{n}{\Delta p}\left[t_k(j) - t_k\big(j|p_k(j) + \frac{1}{n}\Delta p\big)\right], \forall j \neq n.$$

Furthermore, we have the inequality (b) from the gradient property of the convex function [44]. That is, given $h > 0$, the convex function $l(x)$ satisfies

$$l(x+h) - l(h) \geq \lim_{n\to\infty} n[l(x + \tfrac{1}{n}h) - l(h)].$$

(49) illustrates that the AoI of the APP scheme's extreme staleness is always less than that of the EXT scheme's in the worst-case scenario. By substituting $a_k^{(APP)}(n)$ and $a_k^{(EXT)}(n)$ from (4), respectively, we obtain $f_k^{(APP)}(n) \leq f_k^{(EXT)}(n)$.

REFERENCES

[1] Y.-L. Hsu, C.-F. Liu, S. Samarakoon, H.-Y. Wei, and M. Bennis, "Age-optimal power allocation in industrial IoT: A risk-sensitive federated learning approach," in *Proc. IEEE 32nd Annual International Symposium on Personal, Indoor and Mobile Radio Communications (PIMRC)*, Sep. 2021, pp. 1323–1328.

[2] E. Adi, A. Anwar, Z. A. Baig, and S. Zeadally, "Machine learning and data analytics for the iot," *Neural Computing and Applications*, pp. 1–29, 2020.

[3] B. Chang, L. Zhang, L. Li, G. Zhao, and Z. Chen, "Optimizing resource allocation in urllc for real-time wireless control systems," *IEEE Transactions on Vehicular Technology*, vol. 68, no. 9, pp. 8916–8927, 2019.

[4] S. Kaul, M. Gruteser, V. Rai, and J. Kenney, "Minimizing age of information in vehicular networks," in *Proc. 8th Annu. IEEE Commun. Soc. Conf. Sensor, Mesh Ad Hoc Commun. Netw.*, Jun. 2011, pp. 350–358.

[5] C.-F. Liu and M. Bennis, "Taming the tail of maximal information age in wireless industrial networks," *IEEE Commun. Lett.*, vol. 23, no. 12, pp. 2442–2446, Dec. 2019.

[6] B. Zhou and W. Saad, "Age of information in ultra-dense IoT systems: Performance and mean-field game analysis," *CoRR*, vol. abs/2006.15756, pp. 1–30, Jun. 2020.

[7] ——, "Performance analysis of age of information in ultra-dense internet of things (iot) systems with noisy channels," *IEEE Transactions on Wireless Communications*, vol. 21, no. 5, pp. 3493–3507, 2022.

[8] J. Li, Y. Zhou, and H. Chen, "Age of information for multicast transmission with fixed and random deadlines in iot systems," *IEEE Internet of Things Journal*, vol. 7, no. 9, pp. 8178–8191, 2020.

[9] C. Xu, H. H. Yang, X. Wang, and T. Q. S. Quek, "Optimizing information freshness in computing-enabled iot networks," *IEEE Internet of Things Journal*, vol. 7, no. 2, pp. 971–985, 2020.

[10] Y. Lu, K. Xiong, P. Fan, Z. Zhong, and K. B. Letaief, "Online transmission policy in wireless powered networks with urgency-aware age of information," in *Proc. 15th Int. Wireless Commun. Mobile Comput. Conf.*, Jun. 2019, pp. 1096–1101.

[11] A. Elgabli, H. Khan, M. Krouka, and M. Bennis, "Reinforcement learning based scheduling algorithm for optimizing age of information in ultra reliable low latency networks," in *Proc. IEEE Symp. Comput. Commun.*, Jun. 2019, pp. 1–6.

[12] E. Gindullina, L. Badia, and D. Gündüz, "Average age-of-information with a backup information source," in *Proc. IEEE 30th Annu. Int. Symp. Pers., Indoor Mobile Radio Commun.*, Sep. 2019, pp. 1–6.

[13] M. A. Abd-Elmagid, H. S. Dhillon, and N. Pappas, "Aoi-optimal joint sampling and updating for wireless powered communication systems," *IEEE Transactions on Vehicular Technology*, vol. 69, no. 11, pp. 14 110–14 115, 2020.

[14] B. Zhou and W. Saad, "Minimum age of information in the internet of things with non-uniform status packet sizes," *IEEE Transactions on Wireless Communications*, vol. 19, no. 3, pp. 1933–1947, 2020.

[15] X. Xie, H. Wang, and M. Weng, "A reinforcement learning approach for optimizing the age-of-computing-enabled iot," *IEEE Internet of Things Journal*, vol. 9, no. 4, pp. 2778–2786, 2022.

[16] H. Tang, J. Wang, L. Song, and J. Song, "Minimizing age of information with power constraints: Multi-user opportunistic scheduling in multi-state time-varying channels," *IEEE Journal on Selected Areas in Communications*, vol. 38, no. 5, pp. 854–868, 2020.

$$\begin{aligned}
\Delta a_k(n) &= \sum_{j=1}^{n} t_k\big(j|p_k(j) + \frac{1}{n}\Delta p\big) - \left[\sum_{j=1}^{n-1} t_k(j) + t_k\big(n|p_k(n) + \Delta p\big)\right] \\
&= \sum_{j=1}^{n-1}\left[t_k\big(j|p_k(j) + \frac{1}{n}\Delta p\big) - t_k(j)\right] + \left[t_k\big(n|p_k(n) + \frac{1}{n}\Delta p\big) - t_k\big(n|p_k(n) + \Delta p\big)\right] \\
&\overset{(a)}{\leq} (n-1)\left[t_k\big(n|p_k(n) + \frac{1}{n}\Delta p\big) - t_k(n)\right] + \left[t_k\big(n|p_k(n) + \frac{1}{n}\Delta p\big) - t_k\big(n|p_k(n) + \Delta p\big)\right] \\
&= n\left[t_k\big(n|p_k(n) + \frac{1}{n}\Delta p\big) - t_k(n)\right] - \left[t_k\big(n|p_k(n) + \Delta p\big) - t_k(n)\right] \overset{(b)}{\leq} 0.
\end{aligned} \tag{49}$$

[17] B. Yin, S. Zhang, and Y. Cheng, "Application-oriented scheduling for optimizing the age of correlated information: A deep-reinforcement-learning-based approach," *IEEE Internet of Things Journal*, vol. 7, no. 9, pp. 8748–8759, 2020.

[18] M. A. Abd-Elmagid, H. S. Dhillon, and N. Pappas, "A reinforcement learning framework for optimizing age of information in rf-powered communication systems," *IEEE Transactions on Communications*, vol. 68, no. 8, pp. 4747–4760, 2020.

[19] B. McMahan, E. Moore, D. Ramage, S. Hampson, and B. A. y Arcas, "Communication-efficient learning of deep networks from decentralized data," in *Proc. 20th Int. Conf. Artificial Intell. Statistics*, vol. 54, Apr. 2017, pp. 1273–1282.

[20] W. Y. B. Lim, N. C. Luong, D. T. Hoang, Y. Jiao, Y.-C. Liang, Q. Yang, D. T. Niyato, and C. Miao, "Federated learning in mobile edge networks: A comprehensive survey," *IEEE Commun. Surveys Tuts.*, vol. 22, pp. 2031–2063, 2020.

[21] S. Savazzi, M. Nicoli, M. Bennis, S. Kianoush, and L. Barbieri, "Opportunities of federated learning in connected, cooperative, and automated industrial systems," *IEEE Communications Magazine*, vol. 59, pp. 16–21, 2021.

[22] T. Li, A. K. Sahu, M. Zaheer, M. Sanjabi, A. Talwalkar, and V. Smith, "Federated optimization in heterogeneous networks," in *Proceedings of Machine Learning and Systems*, I. Dhillon, D. Papailiopoulos, and V. Sze, Eds., vol. 2, 2020, pp. 429–450.

[23] P. Kairouz *et al.*, "Advances and open problems in federated learning," *Found. Trends Mach. Learn.*, vol. 14, pp. 1–210, 2021.

[24] X. Qiu, T. Parcollet, D. J. Beutel, T. Topal, A. Mathur, and N. D. Lane, "A first look into the carbon footprint of federated learning," *CoRR*, vol. abs/2010.06537, 2020.

[25] S. Savazzi, S. Kianoush, V. Rampa, and M. Bennis, "A framework for energy and carbon footprint analysis of distributed and federated edge learning," *ArXiv*, vol. abs/2103.10346, 2021.

[26] T. D. Burd and R. W. Brodersen, "Processor design for portable systems," *Journal of VLSI signal processing systems for signal, image and video technology*, vol. 13, no. 2, pp. 203–221, Aug. 1996.

[27] M. Asad, A. Moustafa, T. Ito, and A. Muhammad, "Evaluating the communication efficiency in federated learning algorithms," *Proc. IEEE 24th International Conference on Computer Supported Cooperative Work in Design (CSCWD)*, pp. 552–557, 2021.

[28] H. H. Yang, A. Arafa, T. Q. S. Quek, and H. Vincent Poor, "Age-based scheduling policy for federated learning in mobile edge networks," in *Proc. IEEE Int. Conf. Acoust., Speech Signal Process.*, May 2020, pp. 8743–8747.

[29] Y. Ye, S. Li, F. Liu, Y. Tang, and W. Hu, "Edgefed: Optimized federated learning based on edge computing," *IEEE Access*, vol. 8, pp. 209 191–209 198, 2020.

[30] A. M. Ghosh and K. Grolinger, "Edge-cloud computing for Internet of things data analytics: Embedding intelligence in the edge with deep learning," *IEEE Trans. Ind. Informat.*, vol. 17, no. 3, pp. 2191–2200, Mar. 2021.

[31] C.-F. Liu and M. Bennis, "Federated learning with correlated data: Taming the tail for age-optimal industrial iot," in *Proc. 19th International Symposium on Modeling and Optimization in Mobile, Ad hoc, and Wireless Networks (WiOpt)*, 2021, pp. 1–6.

[32] M. J. Neely, *Stochastic Network Optimization with Application to Communication and Queueing Systems*. San Rafael, CA, USA: Morgan and Claypool, Jun. 2010.

[33] S. Coles, *An Introduction to Statistical Modeling of Extreme Values*. London, U.K.: Springer, 2001.

[34] C. E. Rasmussen and C. K. I. Williams, *Gaussian Processes for Machine Learning (Adaptive Computation and Machine Learning)*. The MIT Press, 2005.

[35] A. B. Atkinson, "On the measurement of inequality," *Journal of Economic Theory*, vol. 2, no. 3, pp. 244–263, Sep. 1970.

[36] S. Batewela, C.-F. Liu, M. Bennis, H. A. Suraweera, and C. S. Hong, "Risk-sensitive task fetching and offloading for vehicular edge computing," *IEEE Commun. Lett.*, vol. 24, no. 3, pp. 617–621, Mar. 2020.

[37] T. Lipp and S. Boyd, "Variations and extension of the convex–concave procedure," *Optimization and Engineering*, vol. 17, Jun. 2016.

[38] J. Duchi, E. Hazan, and Y. Singer, "Adaptive subgradient methods for online learning and stochastic optimization," *J. Mach. Learn. Res.*, vol. 12, p. 2121–2159, Jul. 2011.

[39] D. Jones, M. Schonlau, and W. Welch, "Efficient global optimization of expensive black-box functions," *Journal of Global Optimization*, vol. 13, pp. 455–492, Dec. 1998.

[40] E. Esenogho, K. Djouani, and A. M. Kurien, "Integrating artificial intelligence internet of things and 5g for next-generation smartgrid: A survey of trends challenges and prospect," *IEEE Access*, vol. 10, pp. 4794–4831, 2022.

[41] S. Rath, D. Pal, P. S. Sharma, and B. K. Panigrahi, "A cyber-secure distributed control architecture for autonomous ac microgrid," *IEEE Systems Journal*, vol. 15, no. 3, pp. 3324–3335, 2021.

[42] 3GPP, "Technical Specification Group Radio Access Network; Study on channel model for frequencies from 0.5 to 100 GHz (Release 16)," 3rd Generation Partnership Project (3GPP), TR 38.901, November 2020, v 16.1.0.

[43] J. Kwak, Y. Kim, J. Lee, and S. Chong, "DREAM: Dynamic resource and task allocation for energy minimization in mobile cloud systems," *IEEE J. Sel. Areas Commun.*, vol. 33, no. 12, pp. 2510–2523, Dec. 2015.

[44] M. GRASMAIR, "Basic properties of convex functions," 2016.

Yung-Lin Hsu (S'16) is a Ph.D. candidate at the Graduate Institute of Communication Engineering, National Taiwan University, Taiwan. He received his B.S. and M.S. degrees from the Department of Communications, Navigation and Control Engineering, National Taiwan Ocean University, Taiwan. He was a visiting researcher at the Centre for Wireless Communications, University of Oulu, Finland, from 2020 to 2021. His main research interests are 6G and beyond heterogeneous wireless communications, including vehicular-to-everything communications (V2X), smart factory and industrial IoT (IIoT) communication systems, and terrestrial and non-terrestrial network collaboration.

Chen-Feng Liu (S'17–M'22) received the B.S. degree from National Tsing Hua University, Hsinchu, Taiwan, in 2009, the M.S. degree in communications engineering from National Chiao Tung University, Hsinchu, Taiwan, in 2011, and the Ph.D. degree in communications engineering from the University of Oulu, Oulu, Finland, in 2021. In 2012, he joined Academia Sinica, Taipei, Taiwan, as a Research Assistant. He is currently a Researcher with Technology Innovation Institute, Abu Dhabi, UAE. His current research interests include 6G communications, ultra-reliable low-latency communications, and wireless artificial intelligence.

Hung-Yu Wei (Senior Member, IEEE) received his B.S. degree in electrical engineering from National Taiwan University in 1999 and his M.S. and Ph.D. degrees in electrical engineering from Columbia University in 2001 and 2005, respectively. He is a Professor and Interim Department Chair in Department of Electrical Engineering, National Taiwan University. His research interests include next-generation wireless, IoT, and fog/edge computing. He is an Associate Editor for IEEE System Journal and IEEE Internet of Things Magazine. He serves as a Program Co-Coordinator for Taiwan's MOST 6G program. He is currently the Chair of the IEEE P1935 working group for edge/fog management and orchestration standard.

Mehdi Bennis (S'07–AM'08–SM'15–F'21) received the M.Sc. degree from the École Polytechnique Fédérale de Lausanne, Switzerland and the Eurecom Institute, France, in 2002, and the Ph.D. degree in electrical engineering in 2009. He is currently a tenured Full Professor with the Centre for Wireless Communications, University of Oulu, Finland, and head of the intelligent connectivity and networks/systems group (ICON). His main research interests are in radio resource management, heterogeneous networks, game theory and distributed machine learning in 5G networks and beyond. He has published more than 200 research papers in international conferences, journals and book chapters. He has been the recipient of several prestigious awards including the 2015 Fred W. Ellersick Prize from the IEEE Communications Society, the 2016 Best Tutorial Prize from the IEEE Communications Society, the 2017 EURASIP Best paper Award for the Journal of Wireless Communications and Networks, the all-University of Oulu award for research, the 2019 IEEE ComSoc Radio Communications Committee Early Achievement Award and the 2020-2021 Clarviate Highly Cited Researcher by the Web of Science. Dr Bennis is an editor of IEEE TCOM and Specialty Chief Editor for Data Science for Communications in the Frontiers in Communications and Networks journal. Dr Bennis is an IEEE Fellow.